Journal of South American Earth Sciences 29 (2010) 685–704

Contents lists available at ScienceDirect

Journal of South American Earth Sciences

journal homepage: www.elsevier.com/locate/jsames

Petrology of mafic and ultramafic layered rocks from the Jaboncillo Valley, Sierra de Valle Fértil, Argentina: Implications for the evolution of magmas in the lower crust of the Famatinian arc

J.E. Otamendi [a,b,*], E. Cristofolini [a,b], A.M. Tibaldi [a,b], F.I. Quevedo [a], I. Baliani [a]

[a] Departamento de Geología, Universidad Nacional de Río Cuarto, X5804BYA Río Cuarto, Argentina
[b] Consejo Nacional de Investigaciones Científicas y Técnicas, Argentina

ARTICLE INFO

Article history:
Received 1 July 2009
Accepted 6 November 2009

Keywords:
Cumulate
Primitive magma
Fractionation
Arcs
Sierras Pampeanas
Famatinian arc

ABSTRACT

This work presents the field setting, petrography, mineralogy and geochemistry of a gabbroic and peridotitic layered body that is lens-shaped and surrounded by gabbronorites, diorites, and metasedimentary migmatites. This body exposed at Jaboncillo Valley is one among several examples of mafic and ultramafic layered sequences in the Sierras Valle Fértil and La Huerta, which formed as part of the lower crust of the Ordovician Famatinian magmatic arc in central-western Argentina. The layered sequence grew at deep crustal levels (20–25 km) within a mafic lower crust. The base of the layered body was detached during the tectonic uplift of the Famatinian lower crust, whereas the roof of the layered body is exposed in the eastern zone. In the inferred roof, olivine-bearing rocks vanish, cumulate textures are less frequent, and the igneous sequence becomes dominated by massive or thinly banded gabbronorites. Mainly based on the petrographic relationships, the inferred order of crystallization in the gabbroic and peridotitic layered sequence is: (1) Cr–Al-spinel + olivine, (2) Cr–Al-spinel + olivine + clinopyroxene + magnetite, (3) Cr–Al-spinel + olivine + plagioclase + magnetite ± orthopyroxene, and (4) Al-spinel + orthopyroxene + amphibole. A strong linear negative correlation between olivine and plagioclase modal proportions combined with field, petrographic and geochemical observations are used to demonstrate that the physical separation of olivine and plagioclase results in rock diversity at scales of a few centimeters to tens of meters. However, the composition of olivine (Fo ~ 0.81) and plagioclase (An > 94%) remains similar throughout the layered sequence. Spinels are restricted to olivine-bearing assemblages, and display chemical trends characteristic of spinels found in arc-related cumulates. Gabbroic and peridotitic layered rocks have trace element concentrations reflecting cumulates of early crystallizing minerals. The trace element patterns still retain the typical features of subduction-related arc magmatism, showing that the process of cumulate formation did not obscure the trace element signature of the parental magma. Using the composition of cumulus minerals and whole-rock chemical trends, we show that the parental magma was mafic (SiO_2 ~ 48 wt.%) with Mg-number around 0.6, and hydrous. The oxygen fugacity (fO_2) of the parental magma estimated between +0.8 and −0.6 log fO_2 units around the fayalite–magnetite–quartz (FMQ) buffer is also characteristic of primitive hydrous arc magmas. The initially high water content of the parental magma allowed amphibole to crystallize as an interstitial phase all over the crystallization evolution of the layered sequence. Amphibole crystallization in the inter-cumulus assemblage gives rise to the retention of many trace elements which would otherwise be incompatible with the mineral assemblage of mafic–ultramafic cumulates. This study shows that there exist strongly mafic and primitive magmas that are both generated and emplaced within the lower crustal levels of subduction-related magmatic arc. Our findings together with previous studies suggest that the Early Ordovician magmatic paleo-arc from central-northwestern Argentina cannot be regarded as a typical Andean-type tectono-magmatic setting.

1. Introduction

The widespread existence of cognate peridotitic and gabbroic nodules in volcanic rocks with igneous crystallization sequence in which olivine, Cr–Al-spinel and clinopyroxene precede plagioclase and amphibole crystallization was taken to reveal that arc

* Corresponding author. Address: Departamento de Geología, Universidad Nacional de Río Cuarto, X5804BYA Río Cuarto, Argentina. Tel.: +54 358 4676198; fax: +54 358 4680280.
E-mail address: jotamendi@exa.unrc.edu.ar (J.E. Otamendi).

0895-9811/$ - see front matter © 2009 Elsevier Ltd. All rights reserved.
doi:10.1016/j.jsames.2009.11.001

magmas experience continuous differentiation while rising through the lithospheric mantle to the lowermost crust (Arculus and Wills, 1980; Conrad and Kay, 1984; Kay and Kay, 1985; Beard and Borgia, 1989). This result was observational prediction of what igneous rock composition might reflect a primitive mantle-derived magma in arcs. At present, growing consensus is for the view that the great majority of the primitive arc magmas crossing the boundary between the lithospheric mantle and the crust are mafic (SiO_2 < 50 wt.%), high-magnesium (MgO ⩾ 10 wt.%, with MgO/MgO + FeO molar ratio commonly >0.65), and hydrous. The idea is not new (Arculus and Johnson, 1978), and was chiefly constructed upon studying cognate nodules of cumulate dunite, peridotite, wehrlite, pyroxenite, and gabbro in arc volcanic rocks. Since the mineral assemblage dominating the crystallization sequence at pressures higher than the first plagioclase appearance would give rise to melts with lower magnesium but higher aluminum than their closer igneous precursor, high-alumina basalts were thought to be derivative magma produced by high pressure fractionation of high-magnesium basalts (Perfit et al., 1980; Crawford et al., 1987; Sisson and Grove, 1993). Phase relationships in the basaltic system under both hydrous and anhydrous conditions were already known (Holloway and Burnham, 1972; Helz, 1973; Baker and Eggler, 1983; Gust and Perfit, 1987), and were broadly supporting inferences made on the basis of cognate nodules.

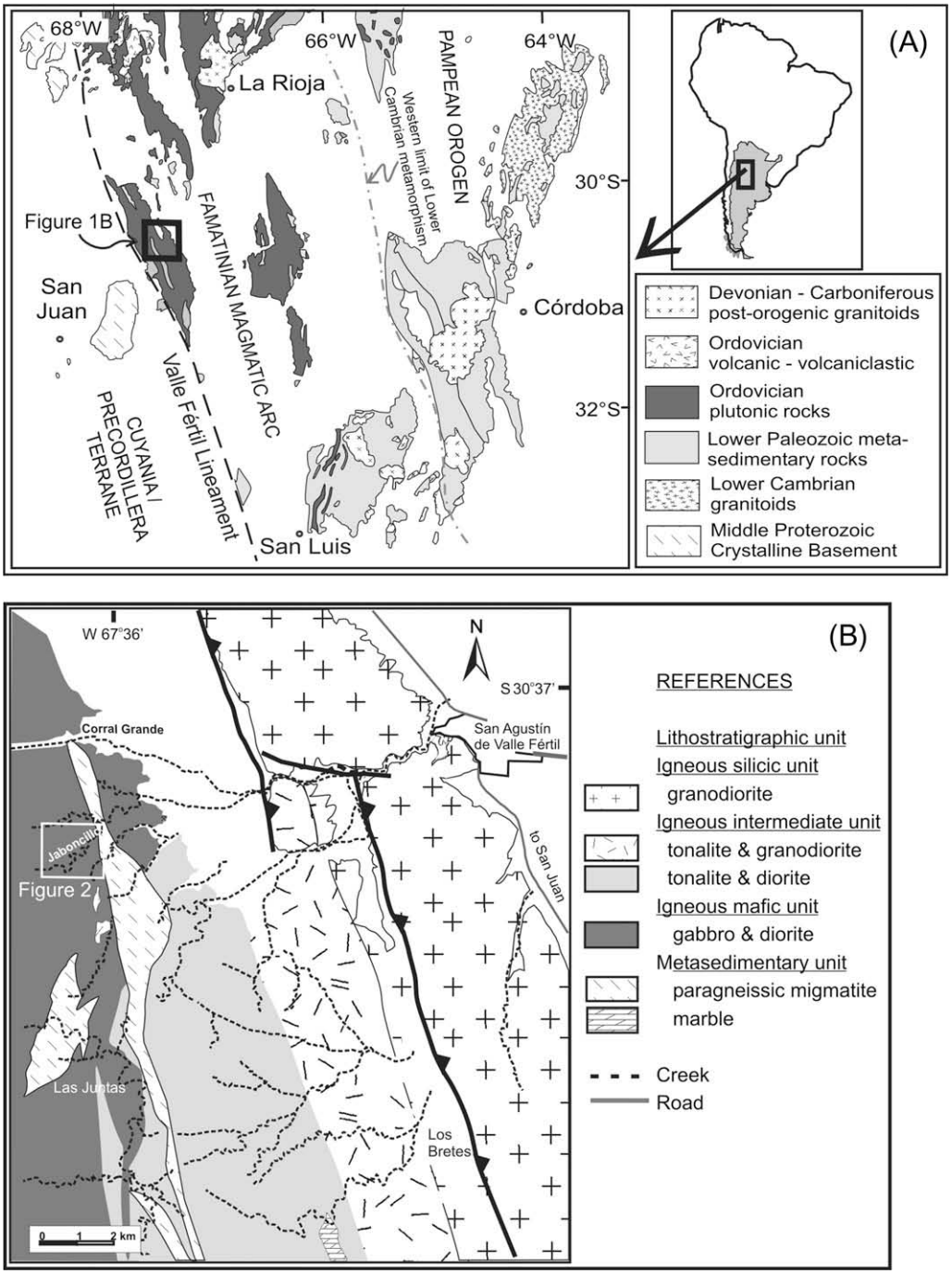

Fig. 1. (A) Map showing the location of the study area with respect to the Pampean orogen, Famatinian magmatic arc and Cuyania and/or Precordillera terrane. This map was modified after Vujovich and Ramos (1999) by using geological information discussed in text. Inset shows the location of the Famatinian arc in Argentina. (B) Simplified geologic map of the Sierras de Valle Fértil taken after the geological maps of Mirré (1976). This also shows the location of the Jaboncillo Valley layered body.

Petrological studies of cognate nodules in volcanic rocks and results from experimental petrology have provided the strongest conceptual framework for understanding deep crustal petrogenesis in arc settings. Nevertheless few natural examples of igneous sequences preserving the crystallization products of hydrous basaltic magmas in the exposed roots of magmatic paleo-arcs have been found (DeBari and Coleman, 1989; DeBari, 1994, 1997; Spandler et al., 2003; Claeson and Meurer, 2004; Jagoutz et al., 2007). Exposures of plutonic sequences crystallized at lower levels of magmatic arcs are significant because neither volcanic cognate nodules nor experimental petrology charges can show the scale at which the petrological mechanism happens in nature.

In this study we focus on a small mafic and ultramafic layered body, which formed in the low crust of the Ordovician Famatinian arc. The body at Jaboncillo Valley is one among several exposures of mafic and ultramafic layered sequences in the Sierras Valle Fértil and La Huerta (Otamendi et al., 2009). The Jaboncillo Valley body was chosen because preserves cumulate crystallization textures in layered sequence of mafic and ultramafic rocks; therefore, it provides an opportunity to study in detail the magmatic processes that occur in the early stages of arc magmatism. Here, we describe the petrology, mineralogy and geochemistry of layered rocks, in order to estimate the physico-chemical conditions under which the cumulate formed, and discuss the geochemical evolution of the parental magmas during formation of the plutonic rock sequence. In this work, we describe a natural case of crystallization of hydrous mafic magmas at moderate depth (*c.* 20–25 km) in an arc-related setting. We show that at these depths magmas feeding the layered sequences have left behind ultramafic assemblages (e.g. Müntener et al., 2001), but are strongly mafic (SiO_2 < 49 wt.%) and hydrous. These rocks may show the first appearance of plagioclase as an early crystallizing phase and massive crystallization of amphibole throughout the late magmatic stage. The significant is that in the magmatic evolutionary trend plagioclase acts as the unique alumina depressor outside the spinel and garnet stability fields. While magmatic amphibole leads to increment silica and

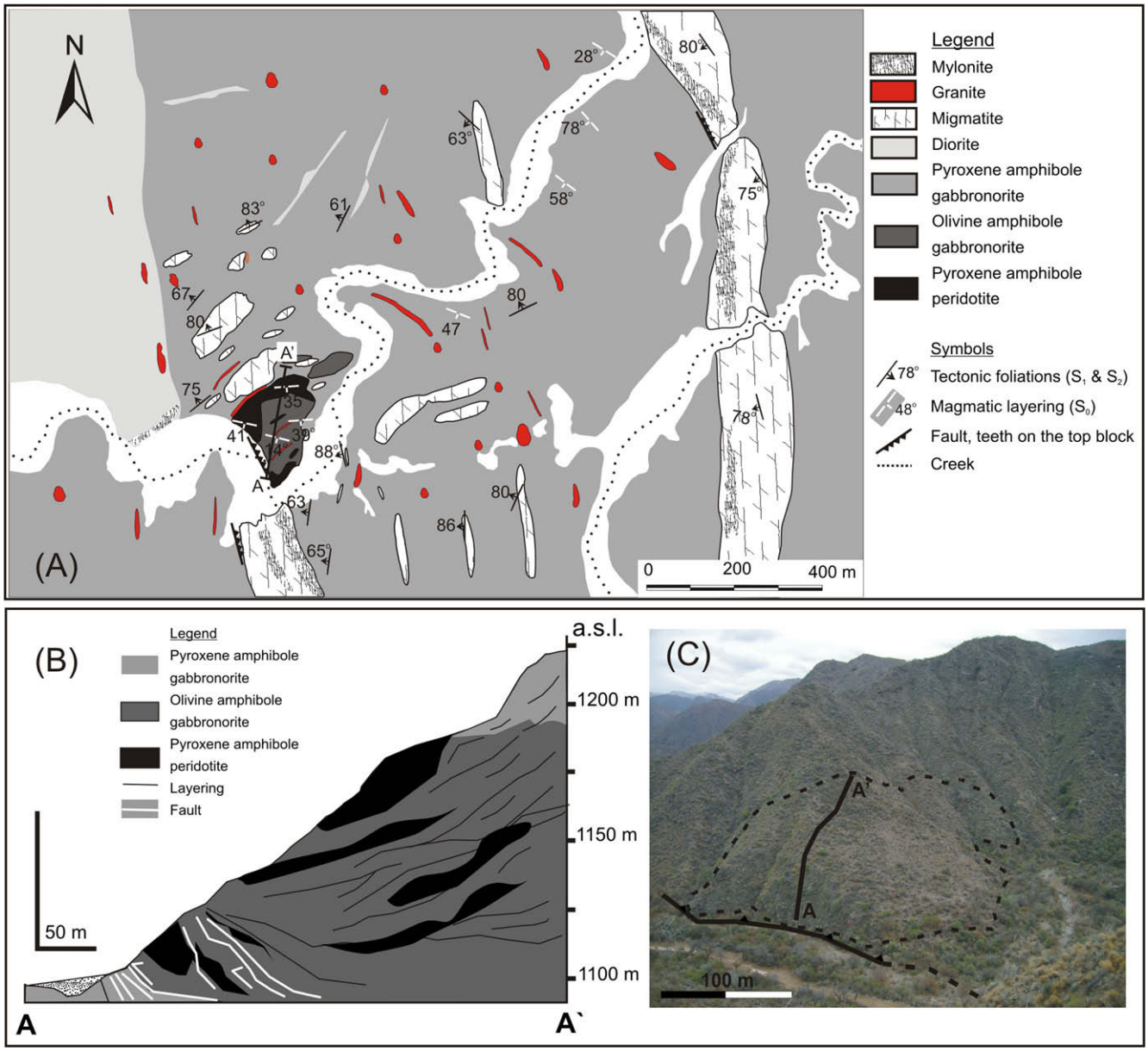

Fig. 2. (A) Geological map of the Jaboncillo Valley based on field mapping. (B) Sketch cross section across the mafic–ultramafic layered body, the line connecting points A and A′ shows the location of this cross section in the geological map. (C) Photograph illustrating the position of the cross section in panel (B) within the layered body that is outlined by a dashed line. The steeply-dipping west-verging shear zone that set the western limit the layered body was observed in the field.

buffer water contents of derivative magmas, as well as has a strong influence on the abundance of incompatible trace elements (Arculus and Wills, 1980; Crawford et al., 1987; Foden and Green, 1992; Gaetani et al., 1993; Claeson and Meurer, 2004; Davidson et al., 2007).

2. Geological Setting

The Famatinian magmatic arc in western Argentina is a differentially exhumed section of an Early to Middle Ordovician arc formed by plate subduction beneath a Gondwanan margin (Toselli et al., 1996; Pankhurst et al., 1998). The Famatinian arc is exposed along more than 1500 km of distance within different segments of the modern central Andean orogen and the transition from plutonic to volcanic Famatinian rocks can be followed over large regions in northwestern Argentina (Toselli et al., 1996; Pankhurst et al., 1998; Coira et al., 1999). The plutonic crustal levels of the Famatinian arc appear as a wide roughly N–S striking belt extending about 600 km between 28°S and 33°S (Fig. 1A). Ordovician eruptive rocks are interbedded with sedimentary rocks in the Puna – Altiplano region between 22°S and 28°S (Coira et al., 1999, 2009) and in the Famatina Mountains (Mannhein and Miller, 1996; Astini and Dávila, 2004). The wall rocks of all the Famatinian plutonic batholiths are metasedimentary packages largely consisting of siliciclastic sediments with subordinate interlayered carbonate beds (Caminos, 1979). As progressively deeper levels of the Famatinian–Puna paleo-arc crust are exposed southward along strike, Neoproterozoic to Early Ordovician stratigraphic units that predated the Famatinian subduction-related magmatism are continuously mapped from non- to weakly-metamorphosed sedimentary rocks in the Puna to regional aureole metasedimentary rock in the central Sierras Pampeanas (Aceñolaza et al., 2000). Epizonal granitoid plutons in the Famatina Mountains and neighboring areas intruded into the early Ordovician volcano-sedimentary sequences, which were deposited coeval with the early magmatic arc stage (Toselli et al., 1996; Astini and Dávila, 2004).

The Valle Fértil mafic–intermediate plutonic complex, Ordovician in age (Pankhurst et al., 2000, and unpublished data), is located in the western region of the Famatinian magmatic arc, within the Sierras Pampeanas of northwestern Argentina (Fig. 1B). The Sierra Valle Fértil section is almost entirely magmatic with minor framework of migmatitic metasedimentay rocks that were metamorphosed and partially melted during magmatism. Consequently, there are no stratigraphic relationships, and hence mapping in the area is based entirely on magmatic way up indicators, metamorphic thermobarometry and grouping of broad rocks types into "units" that predominate at various levels. As proposed by Otamendi et al. (2009) the rock units are: (1) A mafic unit dominated by amphibole gabbronorites and Qtz-bearing diorites, and including mafic and ultramafic Ol-bearing cumulate rocks (symbols for minerals after Kretz, 1983). (2) An intermediate unit comprising an extremely heterogeneous suite of Amph-rich and Bt-bearing tonalites. (3) A granodioritic igneous unit made up by Bt- ± Amph-bearing granodiorites that at regional scale form a batholith (Fig. 1B). In the Sierra Valle Fértil, emplacement of voluminous tonalites and granodiorites took place between 482 and 465 Ma during the most active magmatic time in the Famatinian arc (e.g. Pankhurst et al., 2000; and unpublished data). (4) A metasedimentary unit dominated by paragneissic migmatites (metatexite ≫ diatexite) that occur as km-long belts intercalated with mafic and intermediate igneous rocks or appear widespread

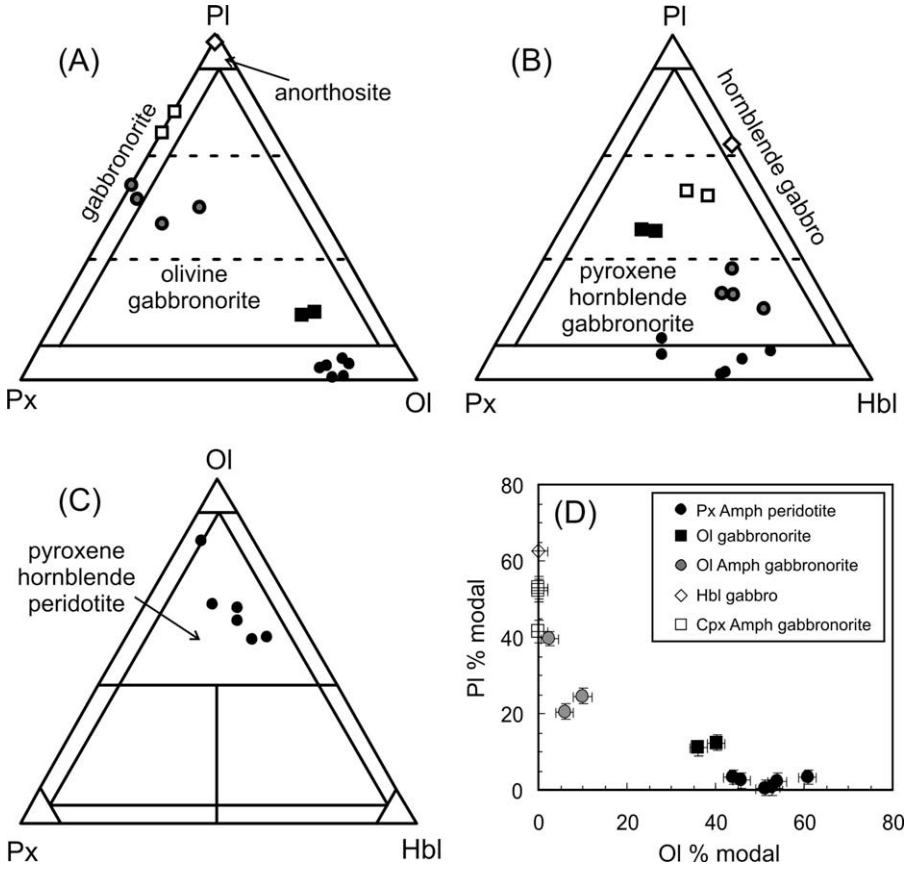

Fig. 3. (A–C) Classification of rock types with the proposal of the commission for igneous rocks systematics (e.g. Le Maitre, 1989). (D) Plot of olivine against plagioclase mineral modal proportions for mafic and ultramafic layered rocks in the Jaboncillo Valley body.

as m-long fragments in all three igneous units. Among metasedimentary rocks, only thick beds of quartzo-feldspathic gneisses do not show any evidence of having experienced partial melting during the thermal metamorphic peak (Otamendi et al., 2008). Instead, most metasedimentary migmatites are characterized by a well-developed layering that results from the alternation of Qtz + Bt + Pl ± Grt ± Crd mesosomes and leucogranitic leucosomes. Metapelitic and semipelitic migmatites interlayered in the mafic unit record peak metamorphic pressures between 5.2 and 7.1 kbar at granulite-facies temperatures of around 805 ± 35 °C (Otamendi et al., 2008).

3. Local geology

Within the Sierra de Valle Fértil we have found several layered bodies containing complete sequence of mafic plutonic rocks with subordinate ultramafic layers. In particular, the layered body that outcrops in the Jaboncillo Valley contains one of the most complete petrological sequences (Mirré, 1976). The gabbroic and peridotitic layered body from the Jaboncillo Valley is a lens-shaped body surrounded by diorites, gabbronorites and metasedimentary migmatites (Fig. 2A). During uplift to the present erosion level, the igneous and metamorphic rocks have been tilted through more than 50°, so that the well-preserved, mafic and ultramafic layered sequence is moderately-dipping and provides a cross-sectional view (Fig. 2B and C).

The body from the Jaboncillo Valley has a tectonic boundary zone all along its western limit (Fig. 2A and B). A brittle-ductile narrow shear zone defines this boundary, and structural features show that the mafic–ultramafic body was tectonically carried onto dioritic rocks and metasedimentary migmatites. In the eastern section, the layered sequence gradationally passes through two-pyroxene gabbros to amphibole gabbronorites. Further towards the east of the layered body, olivine is absent, cumulate textures are less frequent, and the igneous sequence becomes dominated by massive or thinly banded gabbronorites. All these observations reveal that the upper boundary zone of the gabbroic and peridotitic layered body is located on the eastern side. Thus, the lowest structural levels appear in the western and southwestern part, where the layered suite is in tectonic contact with migmatites and diorites (Fig. 2A).

The rock types were distinguished on modal proportion basis (Fig. 3A–C). Pyroxene amphibole peridotite is the dominant rock type in the core of the mafic and ultramafic body. Whereas, the outer parts of the layered body mostly consists of olivine amphibole gabbronorites. Plagioclase-rich amphibole gabbros occur as thin discontinuous layers, and two-pyroxene gabbronorites appear in the upper parts but are barely interbedded within the modally layered sequence. The thickness of a layer, which is determined by being modally homogenous at hand-specimen scale, usually varies from less than ten centimeters to few meters (Fig. 4A). The boundary among layers is generally sharp and marked by the significant change of plagioclase proportion (Fig. 4B), but, in detail, the contact between layers spreads over a few millimeters, indicating that the transition reflects original cumulate processes.

The smooth linear negative correlation between olivine and plagioclase modal proportions (Fig. 3D) combined with field observations suggests that physical separation of olivine and plagioclase renders rock diversity from few centimeters to tens of meters scales. In the great majority of the olivine-bearing rock the modal proportion of olivine + plagioclase adds up to 50 ± 6%. Irrespective of the rock type, amphibole has modal proportion between 20% and 30%. Contrasting with amphibole modal variation, the abundance of orthopyroxene is higher in the olivine amphibole gabbronorites (13–20%) than in the pyroxene amphibole peridotites

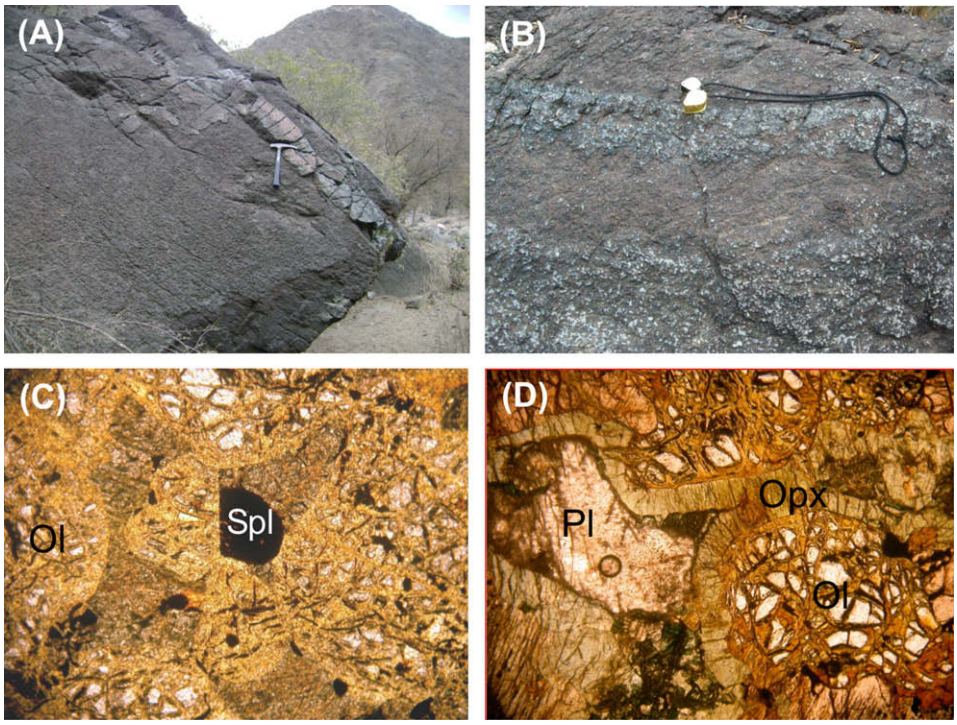

Fig. 4. (A) Photograph of a few-m-thick pyroxene amphibole peridotite that shows a 20-cm thick layer of olivine amphibole gabbronorite. The boundary between rock types is here sharp. (B) Photograph illustrating an example of gradational transition between olivine-dominated and plagioclase-dominated layers. (C) Photomicrograph of an olivine-dominated cumulate rock with pyroxene filling the inter-cumulus. Note that a subhedral crystal of Cr-bearing spinel is overgrowing the cumulus–inter-cumulus boundary, suggesting that some Cr-bearing spinels grew after the cumulate framework was formed. Olivine is mostly altered to serpentine. (D) Photomicrograph of a thin corona of orthopyroxene continuously riming olivine and separating olivine from plagioclase. Photomicrographs (C and D) were obtained under plane-polarized light and their long dimension is ~1.5 mm.

(11 ± 2%). The total amount of oxides (spinel + magnetite) is between 11% and 15% in peridotites and around 10% in the typical gabbronorites.

4. Petrography

4.1. Pyroxene amphibole peridotite

Euhedral or subhedral grains of cumulus olivine are present through the pyroxene amphibole peridotites in dominating amounts (Ol > 40 vol.%). In effect, the main framework-forming phase is always olivine (Fig. 4C), with pyroxenes (orthopyroxene ± clinopyroxene) commonly forming, irregular polymineralic, rims that surround cumulus olivine. Pyroxenes, amphibole, plagioclase, oxides, pleonaste (green spinel) and picotite (Cr-rich Al-spinel) are inter-cumulus phases. Orthopyroxene occurs as an irregularly distributed inter-cumulus phase or monocrystalline continuous rims around cumulus olivine grains. Brownish picotite occurs as euhedral grains enclosed in olivine, or appears intergrowth with pyroxenes as subhedral discrete grains. Plagioclase is concentrated in clusters, and irregularly distributed in the inter-cumulus of olivine orthocumulate rocks. Calcic amphibole occurs as magmatic inter-cumulus grains. Alteration includes the development of patchy, fibrous and veins of serpentine plus oxides within cumulus olivine.

4.2. Olivine amphibole gabbronorite

Because of the variable modal proportions of plagioclase, the olivine amphibole gabbronorites are internally layered (Fig. 4B). Primary igneous minerals are olivine, plagioclase, chromian magnetite and picotite (Cr-rich Al-spinel), whereas orthopyroxene, amphibole, and pleonaste (Cr-poor Al-spinel) may mainly be the reaction products of igneous phases and inter-cumulus melt (Fig. 4D). Large amphibole grains (up to 3 cm in length) forms oikocrysts, and include randomly oriented plagioclase plus olivine grains, which are smaller than those outside the oikocrysts (Fig. 5A). Green spinel (pleonaste) is both intergrowth with amphibole in simplectites and discrete subhedral grains spatially related to picotite (Fig. 5B). Secondary Fe-rich oxides, chlorite and serpentine are found as patches and in cracks from cumulus olivine. No zoning is observed in any of the rock-forming minerals and clinopyroxene is commonly absent in most samples.

This rock type shows the most complete sequence of reaction textures developed between olivine and plagioclase grains. The typical sequence of reaction rims in an olivine–plagioclase corona is: olivine; orthopyroxene, amphibole, symplectic intergrowth of amphibole and pleonaste (green spinel) in direct contact with plagioclase (Fig. 5C). In some reaction rims the orthopyroxene layer is absent (Fig. 5D). Some plagioclase grains with high aspect ratio are bent, with deformation twins, but these features are more common in the lowest parts of the banded sequence (western contact in Fig. 2).

4.3. Amphibole gabbro (anorthosite)

Within this rock type the main framework-forming mineral is plagioclase, which comprises sub-equant to elongate grains with random orientation or a weak mineral preferred orientation alignment. Subhedral amphibole grains are set in coarse-grained plagioclase mosaic. Olivine is absent in such plagioclase-rich gabbroic layers, whereas green spinel appears as blebs forming symplectites

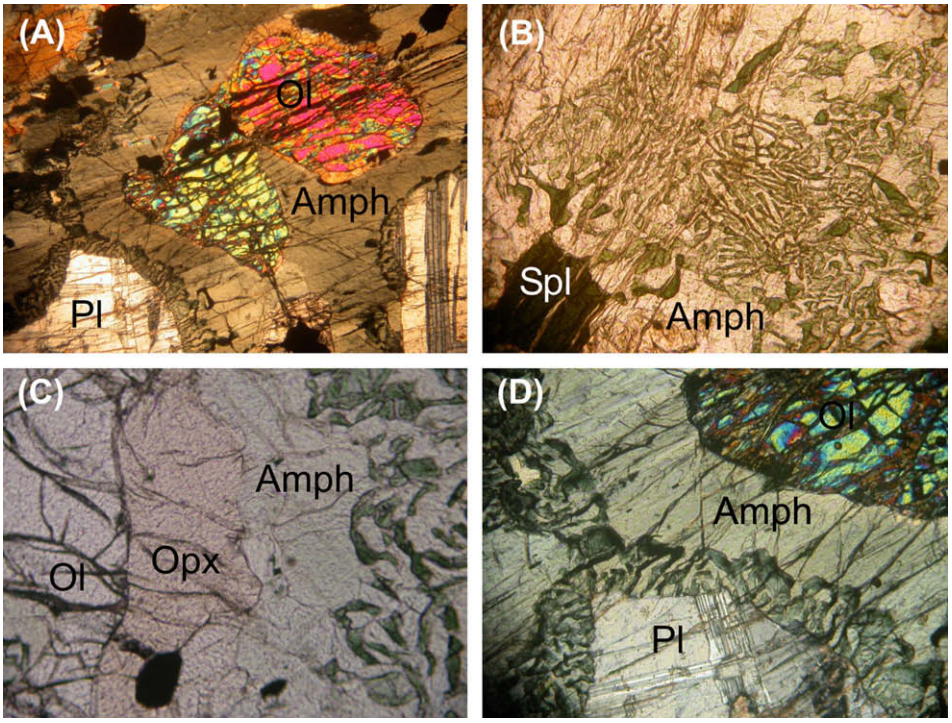

Fig. 5. (A) Photomicrograph showing an amphibole oikocryst. Amphibole grew forming few-cm-long grains that are optically continuous and can be completely observed in hand-size specimens. These amphibole oikocrysts include all of the other minerals in the assemblage, indicating that amphibole grew at late- or post-magmatic stages (cross-polarized light with a long dimension of ~2.5 mm). (B) Photomicrograph of amphibole-spinel symplectite. Spinel appears as worm-like inclusions that spread over large parts of amphibole crystals. Note also that spinels with different contents of Cr are distinguished by their colours; spinels with high Cr contents look dark brownish and form large discrete grains (i.e. at the bottom on the left side of the photograph). (C) Photomicrograph of the olivine–plagioclase corona showing an inner rim of orthopyroxene and an outer rim of amphibole + spinel symplectite. Photomicrographs (B and C) were obtained under plane-polarized light and cover a long dimension of ~1.5 mm. (D) Detail of microphotograph in panel (A) to show that the orthopyroxene rim around olivine was in some cases replaced by amphibole, and that the amphibole-spinel sympletite was mainly formed along the borders of early plagioclase grains (cross-polarized light with a long dimension of ~1.5 mm). (For interpretation of the references to colour in this figure legend, the reader is referred to the web version of this article.)

with amphibole. Locally laths of biotite with weak pleocroism pseudomorphically replaced the boundary of amphibole grains.

4.4. Clinopyroxene-bearing amphibole gabbronorite

This rock type appears in the upper part of the mafic–ultramafic body, but is generally outside the layered sequence. The rocks comprise medium-grained two-pyroxene gabbronorites with 40–60% of plagioclase, variable proportions of amphibole and oxides. Occasionally, these gabbronorites display banding defined by the alternation of plagioclase-rich and plagioclase-poor bands at millimeter scales. Both pyroxenes appear incompletely rimmed by amphibole. Orthopyroxene shows pink–green pleocroism, is subhedral and equant. Clinopyroxene develops large irregular grains, is always less abundant than orthopyroxene and is even absent in some rocks.

5. Composition of minerals

About 200 spot analyses of cumulate minerals were made using a JEOL JXA-8200 Superprobe equipped with four wavelength dispersive X-ray spectrometers that is housed at the University of Huelva, Spain. Analytical conditions for both single spot analyses and X-ray maps are described in Otamendi et al. (2008). Table 1 provides a summary of the compositional range measured in minerals of the distinct rock types.

Olivines are chrysolite with forsterite contents of 78–82%. In general, olivine has two remarkable compositional characteristics, these are: (1) no zoning was detected at crystal scale, and more important (2) the composition is fairly constant throughout the cumulate sequence.

In the olivine-bearing rocks, plagioclase has a high anorthite content that varies between 94% and 99% and is chemically unzoned. According to the compilation of Beard (1986), the composition of plagioclase coexisting with olivine is typical and characteristic of arc cumulate suites (Fig. 6A). Plagioclase often occurs as reabsorbed grains included in amphibole, and these grains have compositions similar to those of cumulus-forming crystals. In the olivine-absent assemblage of the clinopyroxene amphibole gabbronorite, plagioclase has slightly lower anorthite content (89–92%). Within a layer having a plagioclase modal proportion of around 63%, the composition of plagioclase (An $\sim$ 96%) is similar to those of layers dominated by olivine.

Table 1
Representative mineral analyses for the Jaboncillo Valley layered rocks.

Rock	Sample	Mineral	SiO_2	TiO_2	Al_2O_3	Cr_2O_3	FeO	MnO	MgO	CaO	Na_2O	K_2O	Total
Cpx Amph gabbronorite	VFJA4	Opx1	52.48	0.06	2.18		18.67	0.42	24.83	0.25	0.00		98.9
Cpx Amph gabbronorite	VFJA4	Opx14	52.50	0.06	2.20		18.49	0.43	26.47	0.19	0.00		100.3
Cpx Amph gabbronorite	VFJA4	Opx17	52.84	0.08	2.12		18.53	0.41	26.35	0.21	0.02		100.6
Cpx Amph gabbronorite	VFJA4	Cpx27	52.88	0.40	2.93	0.01	5.55	0.37	14.95	22.56	0.31		99.9
Cpx Amph gabbronorite	VFJA4	Cpx28	52.84	0.34	2.84	0.02	5.39	0.40	15.37	22.73	0.37		100.3
Cpx Amph gabbronorite	VFJA4	Cpx29	53.43	0.33	2.26	0.02	6.31	0.31	14.17	23.14	0.33		100.3
Cpx Amph gabbronorite	VFJA4	Pl2	44.59		35.57		0.15			18.33	1.02	0.01	99.7
Cpx Amph gabbronorite	VFJA4	Pl4	44.90		35.46		0.12			18.03	1.25	0.00	99.8
Cpx Amph gabbronorite	VFJA4	Amph5	44.07	1.08	12.64		10.69	0.17	14.26	11.38	1.28	0.62	96.2
Cpx Amph gabbronorite	VFJA4	Amph15	44.81	1.13	11.79	0.05	10.19	0.12	15.642	11.57	1.40	0.72	97.4
Cpx Amph gabbronorite	VFJA4	Amph23	44.23	0.95	12.97	0.04	10.15	0.14	15.393	11.48	1.43	0.58	97.3
Px Amph gabbronorite	VFJA6	Ol1	37.31				18.08	0.24	43.91	0.01			99.5
Px Amph gabbronorite	VFJA6	Ol2	38.60				18.18	0.24	43.29	0.02	0.02		100.3
Px Amph gabbronorite	VFJA6	Opx20	54.12	0.03	2.34		11.90	0.28	30.69	0.32			99.7
Px Amph gabbronorite	VFJA6	Opx21	53.55	0.03	2.96		12.20	0.28	30.41	0.34			99.8
Px Amph gabbronorite	VFJA6	Pl14	42.95		36.10		0.12			19.42	0.35	0.02	99.0
Px Amph gabbronorite	VFJA6	Pl15	43.69		35.94		0.19			19.24	0.52	0.01	99.6
Px Amph gabbronorite	VFJA6	Pl16	43.27		36.25		0.16			19.37	0.42	0.00	99.5
Px Amph gabbronorite	VFJA6	Amph17	44.97	0.29	13.84	0.07	5.83	0.06	17.01	12.51	1.54	0.23	96.3
Px Amph gabbronorite	VFJA6	Amph18	44.75	0.38	13.48	0.08	6.03	0.05	17.72	12.59	1.67	0.23	97.0
Px Amph gabbronorite	VFJA6	Amph28	44.83	0.34	13.67	0.09	5.94	0.06	17.42	12.67	1.74	0.31	97.1
Px Amph gabbronorite	VFJA6	Spl6	0.02	0.07	55.82	4.26	24.55	0.17	13.16	0.01			98.0
Px Amph gabbronorite	VFJA6	Spl9	0.01	0.00	63.66	0.64	19.51	0.13	15.98	0.05			100.0
Px Amph gabbronorite	VFJA7	Ol3	39.00	0.03			17.73	0.25	41.81	0.02	0.01		98.85
Px Amph gabbronorite	VFJA7	Ol12	39.12				18.12	0.24	42.12	0.01			99.61
Px Amph gabbronorite	VFJA7	Ol57	38.90	0.02			18.46	0.13	41.68	0.02	0.01		99.21
Px Amph gabbronorite	VFJA7	Opx10	54.24	0.03	2.69		12.18	0.29	29.21	0.25			98.89
Px Amph gabbronorite	VFJA7	Opx11	55.17		1.82		11.67	0.27	29.83	0.17			98.93
Px Amph gabbronorite	VFJA7	Pl6	42.70		36.61		0.11			19.78	0.08	0.01	99.29
Px Amph gabbronorite	VFJA7	Pl7	42.64		37.50		0.06			19.71	0.03	0.01	99.95
Px Amph gabbronorite	VFJA7	Amph8	45.07	0.26	13.20		7.02	0.05	16.55	12.29	1.70	0.24	96.38
Px Amph gabbronorite	VFJA7	Amph18	46.79	0.12	12.25	0.12	6.31	0.10	16.86	12.31	1.29	0.10	96.25
Px Amph gabbronorite	VFJA7	Amph32	45.64	0.26	12.80	0.10	6.63	0.06	16.76	12.43	1.17	0.29	96.14
Px Amph gabbronorite	VFJA7	Spl16		0.02	57.73	6.29	21.20	0.19	15.05	0.01			100.48
Px Amph gabbronorite	VFJA7	Spl31	0.01	0.02	63.61	0.50	20.89	0.14	14.93	0.05			100.14
Px Amph peridotite	VFJA8	Ol15	39.26	0.02			18.01	0.22	41.81	0.00			99.33
Px Amph peridotite	VFJA8	Ol32	38.61				18.15	0.22	43.29	0.01	0.01		100.28
Px Amph peridotite	VFJA8	Opx10	54.11		3.08	0.01	11.85	0.30	29.61	0.40			99.35
Px Amph peridotite	VFJA8	Opx17	54.19	0.02	3.58	0.01	11.67	0.26	29.54	0.37			99.63
Px Amph peridotite	VFJA8	Opx21	53.83	0.02	3.55		11.82	0.27	29.52	0.39			99.39
Px Amph peridotite	VFJA8	Cpx20	52.78		2.52		4.06	0.14	16.11	23.85	0.11		99.55
Px Amph peridotite	VFJA8	Cpx26	52.56	0.05	2.67	0.02	4.18	0.15	15.80	23.75	0.10		99.29
Px Amph peridotite	VFJA8	Pl1	43.26		36.59		0.15			19.18	0.75	0.02	99.95
Px Amph peridotite	VFJA8	Amph12	44.46	0.54	14.45	0.03	6.50	0.08	16.35	12.70	1.81	0.14	97.05
Px Amph peridotite	VFJA8	Amph29	44.56	0.47	14.68	0.05	6.64	0.08	16.24	12.41	1.79	0.13	97.06
Px Amph peridotite	VFJA8	Spl7	0.05	0.20	41.93	18.17	29.28	0.17	10.05	0.01			99.86
Px Amph peridotite	VFJA8	Spl11	0.03		65.67	0.01	17.43	0.11	16.69	0.02			99.96

The enstatite content of the orthopyroxenes ranges from 77% to 80%, and is similar among all of the olivine-bearing rock types (Fig. 6B). Distinctly, the orthopyroxene of the clinopyroxene-bearing amphibole gabbronorite has enstatite content of around 70%. Clinopyroxene analyzed in a pyroxene amphibole peridotite has wollastonite contents of around 47%, with enstatite ranging from 43% to 45% (Fig. 6B). Whereas clinopyroxene in the amphibole gabbronorite has lower enstatite contents (41–44%) than those of the peridotite, but have similar wollastonite contents (47–48%). In general, clinopyroxenes are moderately aluminous (2.1–3.4 wt.% Al_2O_3) and Ti-poor (<0.4 wt.% TiO_2).

Amphibole and orthopyroxene are the ferromagnesian phases that occur in all of the rock types. However, textures suggest that amphibole is the last rock-forming ferromagnesian mineral to crystallize. The compositions include pargasite, hornblende and tschermakitic hornblende (Fig. 7A). Mg-numbers (e.g. Mg# = Mg/(Mg + Fe^{2+})) of the amphiboles decrease smoothly from the pyroxene amphibole peridotite through olivine-bearing rock types to the clinopyroxene-bearing amphibole gabbronorite (Fig. 7B). As illustrated with Na + K in A sites and total Al (Fig. 7B and C, respectively) the abundance of all the other cations in amphibole remains similar among the distinct rock types.

Magnetite and pleonaste (green spinel) appear in most of the rock types. Whereas Cr-bearing Al-rich spinel (picotite) occurs in olivine-rich rock type, and is scare or absent in olivine-absent mineral assemblages. Picotite is defined for simplicity as those Al-rich spinel with Cr# > 0.1 (where Cr# = Cr/(Cr + Al) cations in octahedral sites). Picotites have Cr/(Cr + Al) ratios of 0.15–0.25 with Mg# ranging between 0.4 and 0.5. By contrast, pleonastes have Cr/(Cr + Al) lower than 0.1 and Mg# around 0.6 (Fig. 8A). Overall, Al–Cr-spinels display the compositional features that have been found in cognate nodules in arc volcanoes and exposures of plutonic cumulate sequences (Fig. 8A and B). The most important characteristics are the compositional trend of decreasing Cr/(Cr + Al) and Fe^{3+}/(Cr + Al + Fe^{3+}) with increasing Mg# (Conrad and Kay, 1984; DeBari and Coleman, 1989; Spandler et al., 2003; Pichavant and Macdonald, 2007). Because of the relatively low Cr

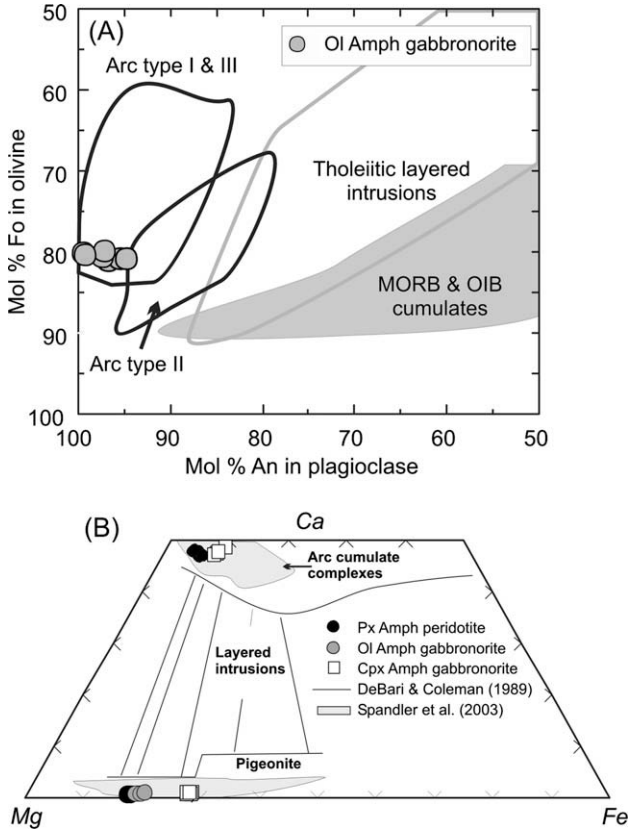

Fig. 6. (A) Compositions of coexisting olivine and plagioclase for mafic and ultramafic layered rocks from the Jaboncillo Valley body. All rock types plot in the field of arc compositions determined by Beard (1986). The field of tholeiitic layered intrusions (grey open line), MORB and OIB cumulates are also taken after Beard (1986). (B) Pyroxene ternary diagram showing the compositions of the mafic and ultramafic layered rocks. Trends for layered intrusion and field for arc cumulates are from DeBari and Coleman (1989) and Spandler et al. (2003).

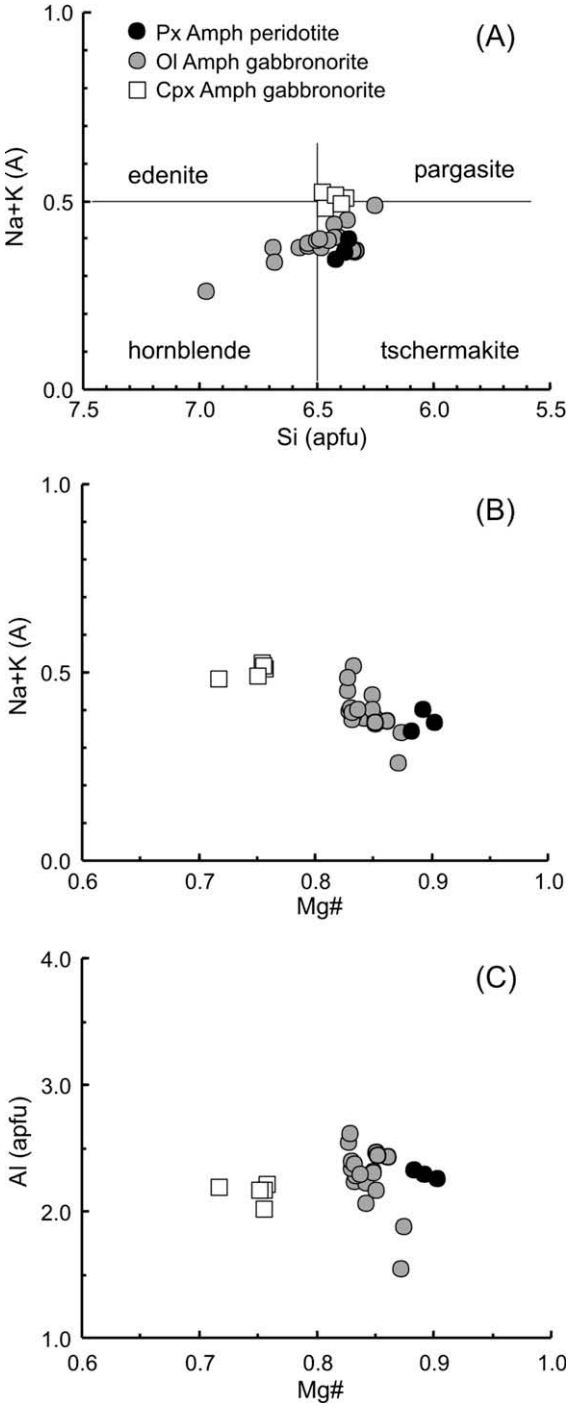

Fig. 7. (A) Classification of the amphiboles based on the Na + K (A) vs. Si in atom per unit formulae concentrations, with nomenclature from Leake et al. (1997). (B) Projection of Na + K cation in A sites vs. Mg-number for amphiboles from the Jaboncillo Valley rocks. (C) Projection of Al atom per unit formulae (apfu) vs. Mg-number.

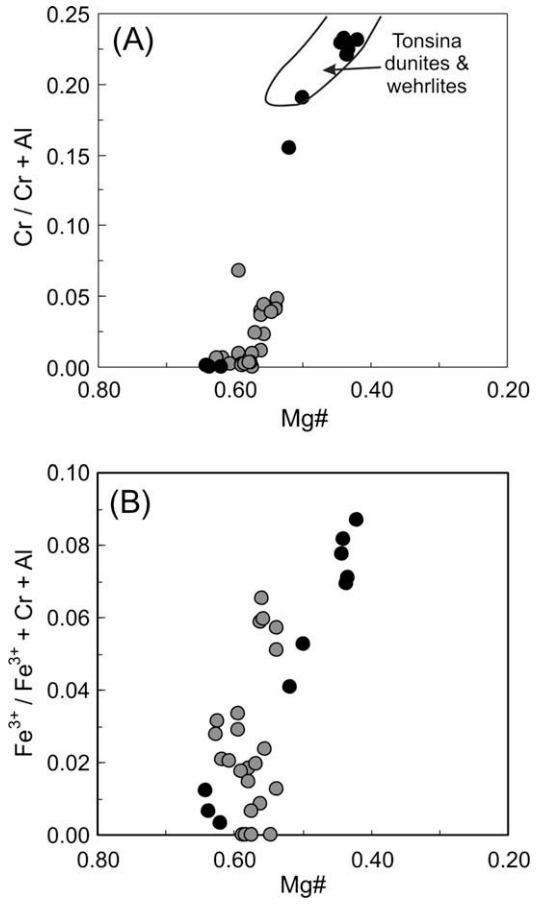

Fig. 8. (A) Cr-number [=Cr/(Cr + Al)] vs. Mg-number for spinel in mafic and ultramafic layered rocks compared with spinel compositional field in the ultramafic from Tonsina (e.g. DeBari and Coleman, 1989). (B) $Fe^{3+}/(Fe^{3+}+Cr+Al)$ ratio vs. Mg-number for spinel from the Jaboncillo Valley body. Symbols as in Fig. 7.

content (Cr_2O_3 < 19 wt.%), picotites from the Jaboncillo Valley body fall in the field of low Cr picotites from lower arc–crustal cumulate (see Conrad and Kay, 1984; DeBari and Coleman, 1989). Whereas, the Cr-poor pleonastes have the same composition as the Al-rich spinels of the gabbroic cumulate from arc settings (e.g. DeBari and Coleman, 1989; Claeson, 1998; Spandler et al., 2003).

Primary magnetite is present within all of the olivine-bearing rocks, but subordinate to Al–Cr-spinels. In the olivine gabbros and peridotites, magnetite contains up to 5 wt.% Cr_2O_3, and is nearly TiO_2 absent (TiO_2 < 0.6 wt.%). In contrast, the magnetite found in clinopyroxene-bearing amphibole gabbronorite is very pure (Mt ~ 98%) in composition and is usually associated with small amounts of ilmenite (Ilm ~ 82%).

6. Temperature, pressure, and oxygen fugacity

6.1. Thermometry

The two-pyroxene thermometer yields the highest temperatures (Table 2). Geothermometer of Wood and Banno (1973), Wells (1977), and Brey and Köhler (1990) give temperatures in the pyroxene amphibole peridotite (VFJA8) around 1200 ± 30 °C and in the clinopyroxene amphibole gabbronorite (VFJA4) from 1060 to 1180 °C (Table 2). These temperatures are regarded as recording close to liquidus crystallization conditions.

Pyroxenes in the peridotitic layers tend to be inter-cumulus crystals of olivine orthocumulates. Since olivine was the liquidus phase, two-pyroxene thermometry indicates that most of the olivine crystallizes at temperatures >1200 °C. This result is consistent with the phase diagram experimentally determined using high-Mg basaltic starting composition and imposing fluid-absent conditions (e.g. Gust and Perfit, 1987). If olivine was extensively crystallized above 1200 °C and at moderate pressures (<8 kbar), the extrapolation of the phase diagram by Pichavant and Macdonald (2007) for a high-Mg magma would result in initial magmatic water content lower than 2 wt.%.

The existence of Cr-rich spinels (picotite) included in olivine cumulus grains or in the olivine inter-cumulus is taken to indicate that picotite closely follow olivine crystallization. However, olivine-spinel thermometry yields unrealistically low temperatures (<600 °C using O'Hara calibration as modified by Ballhaus et al., 1991). Fe–Mg exchange upon cooling must have affected picotite Mg#s, so that olivine-spinel thermometry yields closure temperature for the Fe–Mg ion exchange.

As shown in Table 3, amphibole–plagioclase thermometry (Holland and Blundy, 1994) performed in the mafic and ultramafic rocks yields a wide range of temperature at 6 kbar (which is an average pressure for the Sierra Valle Fértil, Otamendi et al., 2008). Since, all the rocks have highly calcic plagioclase (An ⩾ 90%) and most of them have quartz-absent assemblages, both the edenite–tremolite (A) and edenite–richterite (B) thermometers are not strictly applicable to these rocks and would cause problem for interpreting results. The edenite–tremolite

Table 2
Component activities and calculated temperatures from two-pyroxene thermometry.

		$aMg_2Si_2O_6$(Cpx)	$aMg_2Si_2O_6$(Opx)	lnK	*T* (°C) W&B(73)	*T* (°C) W(77)	Ca^{M2} (Cpx)	Ca^{M2} (Opx)	ln K^*	*P* (kbar)	*T* (°C) B&K(90)
SAMPLE VFJA8 pyroxene amphibole peridotite											
Cpx 20	Opx 10	0.194	0.615	−1.15	**1188**	**1213**	0.471	0.008	−0.629	6	**1230**
Cpx 20	Opx 17	0.194	0.609	−1.14	**1195**	**1219**	0.471	0.007	−0.630	6	**1232**
Cpx 20	Opx 21	0.194	0.611	−1.15	**1190**	**1216**	0.471	0.007	−0.630	6	**1230**
Cpx 26	Opx 10	0.188	0.615	−1.18	**1182**	**1204**	0.471	0.008	−0.629	6	**1230**
Cpx 26	Opx 17	0.188	0.609	−1.17	**1188**	**1210**	0.471	0.007	−0.630	6	**1233**
Cpx 26	Opx 21	0.188	0.611	−1.18	**1184**	**1207**	0.471	0.007	−0.629	6	**1230**
SAMPLE VFJA4 clinopyroxene amphibole gabbronorite											
Cpx 27	Opx 1	0.168	0.469	−1.028	**1085**	**1170**	0.444	0.005	−0.582	6	**1122**
Cpx 27	Opx 14	0.168	0.518	−1.128	**1073**	**1146**	0.444	0.004	−0.584	6	**1137**
Cpx 27	Opx 17	0.168	0.510	−1.113	**1076**	**1151**	0.444	0.004	−0.583	6	**1135**
Cpx 29	Opx 1	0.151	0.469	−1.134	**1066**	**1140**	0.456	0.005	−0.604	6	**1121**
Cpx 29	Opx 14	0.151	0.518	−1.234	**1055**	**1118**	0.456	0.004	−0.604	6	**1136**
Cpx 29	Opx 17	0.151	0.510	−1.219	**1057**	**1122**	0.456	0.004	−0.604	6	**1134**

W&B(73) is for Wood and Banno (1973), W(77) is for Wells (1977), and B&K(90) is for Brey and Köhler (1990). The activity of useful phase components and values of respective equilibrium constants were calculated as suggested by each calibration. Representative mineral composition utilized for performing thermometry are those presented in Table 1.

Table 3
Component concentration and calculated temperatures from hornblende–plagioclase thermometry and pressures from Al-in-hornblende barometry.

		Mg#	An	*P* (kbar)	*T* (°C) H&B/TB	Al(4)	Al(6)	*P* (kbar) J&R(1989)	*P* (kbar) S(1992)
SAMPLE VFJA4 pyroxene amphibole peridotite									
Pl-2	Amph-5	0.70	0.91	6.0	**1021**	1.62	0.54	**4.1**	**5.5**
Pl-3	Amph-15	0.73	0.91	6.0	**1059**	1.60	0.39	**4.1**	**5.5**
Pl-4	Amph-23	0.73	0.89	6.0	**1005**	1.69	0.49	**4.0**	**5.4**
Pl-12	Amph-24	0.73	0.92	6.0	**1053**	1.65	0.48	**4.0**	**5.3**
Pl-13	Amph-25	0.72	0.89	6.0	**1013**	1.68	0.46	**4.0**	**5.4**
Pl-19	Amph-5	0.70	0.90	6.0	**1003**				
Pl-21	Amph-15	0.73	0.91	6.0	**1065**				
SAMPLE VFJA6 olivine amphibole gabbronorite									
Pl-14	Amph-17	0.95	0.97	6.0	**1021**	1.61	0.70	**6.3**	**8.0**
Pl-15	Amph-18	0.97	0.95	6.0	**960**	1.68	0.57	**6.0**	**7.7**
Pl-16	Amph-28	0.96	0.96	6.0	**1012**	1.66	0.61	**6.2**	**7.8**
SAMPLE VFJA7 olivine amphibole gabbronorite									
Pl-26	Amph-28	0.82	0.97	6.0	**1041**	1.40	0.84	**5.9**	**7.5**
Pl-26	Amph-49	0.81	0.97	6.0	**1047**	1.47	0.87	**6.3**	**8.0**
SAMPLE VFJA8 pyroxene amphibole peridotite									
Pl-1	Amph-12	0.93	0.93	6.0	**756**	1.61	0.84	**6.8**	**8.5**
Pl-2	Amph-29	0.91	0.93	6.0	**726**	1.60	0.88	**7.0**	**8.7**
Pl-3	Amph-33	0.91	0.94	6.0	**740**	1.60	0.86	**6.9**	**8.6**

H&BTB is for Holland and Blundy (1994) thermometer (B) based on edenite–anorthite reaction. Mg# is Mg-number for amphibole and An anorthite model fraction of each hornblende–plagioclase pair. J&R(1989) are pressure estimates with calibration after Johnson and Rutherford (1989); and S(1992) are pressures obtained though the calibration by Schmidt (1992). Al(4) and Al(6) are aluminum-in-hornblende concentrations per unit formulae in tetrahedral and octahedral crystal sites, respectively. Representative min-ral composition utilized for performing thermometry are those presented in Table 1.

thermometer yielded unrealistically high temperatures that were disregarded. The Cpx-bearing amphibole gabbronorite (i.e. VFJA4) amphibole–plagioclase thermometry yields results within the range 1031 ± 27 °C (Table 3), where uncertainties are 1σ. A similar range of temperatures are also found in the olivine amphibole gabbronorite (VFJA6 and VFJA6 in Table 3). Amphibole–plagioclase thermometry applied to the pyroxene amphibole peridotite gives temperatures between 720 °C and 750 °C (VFJA8 in Table 3), reflecting that either amphibole crystallized entirely under subsolidus conditions and upon significant cooling, or the small amount of plagioclase in this rock was unable to have influenced the composition of amphibole.

Temperature estimates derived from several amphibole–plagioclase pairs in rocks having olivine-absent and olivine-bearing assemblages (VFJA4, VFJA6, and VFSJ7) indicate that amphibole grew at the lowest magmatic temperatures or close to the subsolidus temperatures. Importantly this observation is consistent with petrographic analysis.

6.2. Barometry

Al-in-hornblende barometry provides the only approach to estimate pressure in the mafic and ultramafic rocks; none of them, however, contains the mineral assemblage hornblende + biotite + plagioclase + quartz + orthoclase + sphene + magnetite/ilmenite required for applying the calibrations by Johnson and Rutherford (1989) and Schmidt (1992).

Pressure calculated through Al-in-hornblende barometry for the Jaboncillo mafic and ultramafic rocks, without exception, yield a wide pressure range of 5.84 ± 1.1 (uncertainty is 1σ) for Johnson and Rutherford (1989) calibration and of 7.46 ± 1.2 (1σ) with Schmidt (1992) geobarometer (Table 3). This study cannot evaluate the origin of the differences between the two Al-in-hornblende geobarometer. However, it is remarkable that results estimated using Johnson and Rutherford (1989) give always lower pressures than those obtained with Schmidt (1992) geobarometer (Table 3). Moreover, both calibrations yield pressure estimates within the pressure range determined in metapelitic migmatites from the nearby Otarola Valley (e.g. Otamendi et al., 2008), which is also consistent with the absence of any major tectonic boundary separating Jaboncillo and Otarola crustal sequences (Fig. 1B). Thus, assuming an average density of 2.8 g/cm^3 for the overlying crustal pile, these pressure estimates indicates crystallization paleodepths between 21 and 27 km for the Jaboncillo Valley mafic–ultramafic body.

6.3. Oxygen fugacity

Results for calculations of fO_2 using coexisting olivine, orthopyroxene and spinel (e.g. Wood et al., 1990; Ballhaus et al., 1991) with the reaction:

$$6Fe_2SiO_4(Ol + O_2(fluid)) \leftrightarrow 3Fe_2Si_2O_6(Opx) + 2Fe_3O_4(Usp) \quad (1)$$

are presented in Table 4. The Fe^{3+} of spinel was estimated imposing stoichiometric and charge balance constraints on electron microprobe analytical data. Because the chief source of error in fO_2 calculations is related to the inaccurate and indirect determination of Fe^{3+} in spinel (see O'Neill and Wall, 1987; Wood and Virgo, 1989), the estimated fO_2 would be taken as provisional approximation. Nevertheless, as shown by Ballhaus et al. (1991) the error derived from using microprobe data yields results that randomly spread over the range of uncertainties generated by the calibration of the fO_2 geobarometer.

The fO_2 calculations are made at equilibration temperatures of 1200 °C as estimated through the coexisting two pyroxenes and at pressure determined from Al-in-amphibole geobarometry. Results are presented relative to the FMQ buffer rendering them essentially insensitive to both temperature and pressure (Wood et al., 1990; Ballhaus et al., 1991). The oxygen fugacities (fO_2) recorded by matching picotites (Cr-spinel) and cumulus olivine range from +0.8 to −0.6 Δlog FMQ units (Table 4).

The standard state of the oxygen buffer reaction:

$$3Fe_2SiO_4 + O_2 \leftrightarrow 3SiO_2 + 2Fe_3O_4 \quad (2)$$

can be estimated using the thermodynamic data base of Berman (1988) at a given *P*–*T* point of interest. Maximum and minimum (+0.8 to −0.6 Δlog FMQ) oxygen fugacites computed at 6 kbar and 1200 °C and expressed as $\log_{10} fO_2$ oxygen fugacities are −6.86 and −8.26, respectively. Using these values of $\log_{10} fO_2$, the theoretical Fe_2O_3/FeO in a mafic magma (i.e. specimen VFJA4 in Table 5)

Table 4
Mineral composition and calculated oxygen fugacitites.

	Spl5	Spl6	Spl8	Spl5	Spl6	Spl8
SAMPLE VFJA6 olivine amphibole gabbronorite						
Al	1.80	1.80	1.80	1.80	1.80	1.80
Cr	0.08	0.09	0.07	0.08	0.09	0.07
Fe^{3+}	0.11	0.10	0.13	0.11	0.10	0.13
Fe^{2+}	0.46	0.46	0.44	0.46	0.46	0.44
Mg	0.54	0.54	0.56	0.54	0.54	0.56
	Ol2	Ol2	Ol2	Ol3	Ol3	Ol3
Fo	0.809	0.809	0.809	0.814	0.814	0.814
T (°C)	1200	1200	1200	1200	1200	1200
P (kbar)	6	6	6	6	6	6
ΔFMQ	**0.50**	**0.31**	**0.69**	**0.55**	**0.36**	**0.47**
	Spl5	Spl6	Spl8	Spl5	Spl6	Spl8
SAMPLE VFJA7 olivine amphibole gabbronorite						
Al	1.80	1.91	1.91	1.80	1.91	1.91
Cr	0.13	0.04	0.05	0.13	0.04	0.05
Fe^{3+}	0.07	0.05	0.04	0.07	0.05	0.04
Fe^{2+}	0.40	0.44	0.43	0.40	0.44	0.43
Mg	0.59	0.56	0.57	0.59	0.56	0.57
	Ol3	Ol3	Ol3	Ol57	Ol57	Ol57
Fo	0.808	0.808	0.808	0.801	0.801	0.801
T (°C)	1200	1200	1200	1200	1200	1200
P (kbar)	6	6	6	6	6	6
ΔFMQ	**−0.63**	**−0.96**	**−1.32**	**−0.56**	**−0.91**	**−1.27**
	Spl5	Spl6	Spl8	Spl5	Spl6	Spl8
SAMPLE VFJA8 pyroxene amphibole peridotite						
Al	1.39	1.44	1.43	1.39	1.44	1.43
Cr	0.42	0.41	0.42	0.42	0.41	0.42
Fe^{3+}	0.17	0.14	0.14	0.17	0.14	0.14
Fe^{2+}	0.58	0.57	0.57	0.58	0.57	0.57
Mg	0.42	0.44	0.43	0.42	0.44	0.43
	Ol5	Ol5	Ol5	Ol6	Ol6	Ol6
Fo	0.801	0.801	0.801	0.805	0.805	0.805
T (°C)	1200	1200	1200	1200	1200	1200
P (kbar)	6	6	6	6	6	6
ΔFMQ	**0.78**	**0.43**	**0.46**	**0.83**	**0.48**	**0.50**

Note that fO_2 values are reported normalized to FMQ buffer and quoted as ΔFMQ, with $\Delta FMQ = [\log (fO_2)^{sample} - \log (fO_2)^{FMQ}]$ at a given *P*–*T* condition.

was estimated with the empirical equation first proposed by Sack et al. (1980) and subsequently modified by Kress and Carmichael (1991). Eq. (6) from Kress and Carmichael (1991) applied within the $CaO–Al_2O_3–Fe_2O_3–FeO–SiO_2$ simple system predicts a range of Fe_2O_3/FeO between 0.11 and 0.22. Simple mass balance calculations based on mineral and whole-rock compositions will be used below to further test the consistency of oxygen barometry estimates obtained though the olivine–orthopyroxene-spinel assemblage.

Cr-bearing magnetite in the olivine-present rocks and magnetite with exsolved ilmenite in the olivine-absent gabbronorites document that most of the Fe–Ti oxide was originally magnetite-ulvospinel solid solution. The almost total lack of magmatic ilmenite would, thereby, be a consequence of differentiation at relatively high fO_2 (Snyder et al., 1993).

7. Sequence of crystallization and generation of the corona texture

Olivine is clearly one of the early crystallizing igneous minerals. Subhedral Cr-rich picotites are found included in olivine. Furthermore, inclusions of clinopyroxene are found in plagioclase and amphibole. Petrographic observations prove plagioclase is a magmatic phase. However, plagioclase crystallized after olivine and most likely after clinopyroxene. The relatively late crystallization of plagioclase accounts for the first appearance of plagioclase in the inter-cumulus of olivine-dominated peridotitic rocks, and hence the low Al_2O_3 whole-rock contents of this rock type (see also Section 8). Locally, coronas are developed where olivine is in contact with plagioclase. Corona textures overprint interstitial amphibole and are interpreted as products of deuteric reactions (Claeson, 1998). Orthopyroxene is mostly rimming cumulus olivine, but is cumulus in the peridotite layers. Accessory Cr-bearing magnetite occurs in early olivine-bearing cumulates. Amphibole is present in all of the rocks, and in some rocks poikilitic amphibole is almost the only interstitial mineral.

Mainly based on the petrographic relationships, the inferred order of crystallization is: (1) Cr–Al-Spl + Ol, (2) Cr–Al-Spl + Ol + Cpx + Mt, (3) Cr–Al-Spl + Ol + Pl + Mt ± Opx ± Cpx, and (4) Al-Spl + Opx + Amph. The last assemblage may have formed when early crystallized olivine and plagioclase reacted with the interstitial liquid to form amphibole (Meurer and Claeson, 2002; Claeson and Meurer, 2004). This idea will be discussed with the generation of corona textures around olivine and plagioclase (see also Baldo et al., 1999). The sequence of crystallization petrophaphically inferred for the Jaboncillo body resembles in many respects the experimental phase diagrams of Gust and Perfit (1987) and Pichavant and Macdonald (2007). This resemblance suggests that the Jaboncillo cumulate rocks formed from a primitive (SiO_2 < 50 wt.% and MgO > 9 wt.%) hydrous magma at pressures between 4 and 10 kbar. Had pressure been below 4 kbar plagioclase would have crystallized preceding clinopyroxene. On the other

Table 5
Whole-rock and moda composition of rock from the Jaboncillo Valley body, Sierra Valle Fértil.

Sample	VFJA4		VFJA58	VFJA64	VFJA55	VFJA63	VFJA7
Rock type	Cpx Amph gabbronorite	Duplicate	Ol Amph gabbronorite	Ol Amph gabbronorite	Amph Px peridotite	Amph Px peridotite	Ol Amph gabbronorite
Major elements (wt.%)							
SiO_2	45.94	46.30	45.07	44.80	38.34	36.96	42.03
TiO_2	0.53	0.49	0.14	0.15	0.13	0.11	0.15
Al_2O_3	17.64	17.55	22.58	21.55	9.62	6.49	19.16
Fe_2O_3	11.19	11.42	5.06	5.89	14.25	15.16	9.41
MnO	0.19	0.19	0.08	0.09	0.18	0.20	0.13
MgO	10.15	10.14	9.04	9.33	25.13	29.24	16.80
CaO	12.81	12.28	15.85	16.08	5.34	3.73	10.73
Na_2O	0.61	0.62	0.75	0.58	0.34	0.29	0.53
K_2O	0.13	0.12	0.14	0.09	0.21	0.11	0.07
P_2O_5	0.01	0.03	0.02	0.02	0.06	0.05	0.02
LOI	0.50	0.60	0.90	1.10	5.70	6.90	1.18
Total	99.70	99.74	99.63	99.68	99.30	99.24	100.21
Mineral modal proportion							
Ol + Srp	0		10	16	44	51	6
Opx	17		14	11	8	11	15
Cpx	15		0	0	1	3	4
Amph	23		38	39	29	22	44
Pl	42		25	24	3	0	21
Spl	0		11	7	8	4	9
Mt	3		2	3	7	8	1
Trace elements (ppm)							
Li	6.9		3.8	9.3	3.1	4.6	
Be	0.4		0.2	0.2	0.2	0.2	
B	80.5		89.5	116.5	78.9	78.8	
Cs	0.1		0.1	0.1	0.5	0.1	
Sc	62.6		46.6	49.0	19.0	17.4	
V	318.0		109.0	101.0	80.0	70.0	
Cr	168.8		810.1	706.3	679.2	671.8	
Co	47.0		31.8	39.2	128.3	138.6	
Ni	77.0		138.0	145.0	595.0	680.0	
Cu	165.0		59.9	169.3	45.2	65.0	
Zn	9.0		4.0	5.0	13.0	17.0	
Ga	15.5		12.6	13.4	5.5	4.2	
Rb	2.7		2.3	1.8	6.7	2.7	
Ba	30.0		39.0	27.0	37.0	22.0	
Sr	145.8		187.6	185.0	86.7	71.7	
Y	7.70		3.60	3.80	3.10	2.20	
Zr	27.0		26.3	61.2	24.3	51.5	
Nb	1.0		0.7	0.2	1.1	0.6	
La	2.60		1.40	1.70	2.50	2.10	
Ce	6.70		3.50	4.00	5.30	4.30	
Pr	1.01		0.50	0.55	0.69	0.53	
Nd	5.00		2.10	2.10	2.70	2.00	
Sm	1.23		0.55	0.65	0.55	0.45	
Eu	0.39		0.24	0.22	0.17	0.14	
Gd	1.24		0.66	0.67	0.52	0.39	
Tb	0.23		0.11	0.13	0.10	0.07	
Dy	1.33		0.61	0.68	0.55	0.38	
Ho	0.28		0.13	0.15	0.11	0.08	
Er	0.89		0.35	0.40	0.30	0.23	
Tm	0.12		0.06	0.06	0.05	0.04	
Yb	0.73		0.35	0.36	0.30	0.26	
Lu	0.12		0.05	0.06	0.05	0.04	
Hf	0.62		0.65	4.00	0.63	1.05	
Ta	0.12		0.07	0.07	0.04	0.11	
Pb	1.79		1.38	5.25	3.07	3.06	
Th	0.29		0.25	0.57	0.87	0.37	
U	0.04		0.08	0.18	0.21	0.14	

Total Fe reported as $Fe_2O_3^*$. For this reason Mg# is MgO/(MgO + FeO) on molar basis but after converting $Fe_2O_3^*$ to FeO^*. Modal proportion was determined by point counting (1200–2000 points). Composition of sample VFJA7 is taken after Otamendi et al. (2009).

side, pressure higher than 10 kbar would have precluded olivine to be the liquidus phase.

In their study of the Mt. Moffett volcano cognate nodules, Conrad and Kay (1984) showed that the sequence of crystallization varies from ultramafic to mafic rocks. If separated by rock types, the sequence of crystallization in the Jaboncillo Valley body resembles in every respects with those deduced by Conrad and Kay (1984). The relevance of this realization is that cumulate layered body from the Jaboncillo Valley would expose on the Earth's surface the predicted composition of arc lower crust as several studies inferred from studying cognate nodules in arc volcanoes (e.g. Arculus and Wills, 1980; Kay and Kay, 1985; DeBari et al., 1987; among others).

This work is not aimed at unraveling the causal mechanisms that explain corona formation in the Jaboncillo Valley rocks. This issue is too controversial to be treated in a work that pursues as

ultimate goal presenting a new exposure of hydrous mafic cumulate sequence. There exist excellent reviews about what studies of corona reaction textures have shown over the years (e.g. Johnson and Carlson, 1990; among many others). Here, we describe the most notorious petrographic and compositional features of minerals involved as reactant and product of the corona-forming mechanism just to set the problem for its resolution in the studied gabbroic cumulates. Compare with world-wide found examples of coronitic gabbros, the most distinctive characteristic of this particular case is that nearly anorthite-pure plagioclase was a reactant of the corona-forming reaction. Coronas in gabbroic cumulate from the Jaboncillo Valley are well-organized reactions texture consisting commonly of two layers between plagioclase and olivine (Fig. 9). On the plagioclase side the layer consists of either amphibole + pleonaste symplectite or amphibole. The other layer appears incompletely surrounding olivine and is made up by pure orthopyroxene. Textural relationships indicate that orthopyroxene grew at the expense of olivine, whereas amphibole partly overgrew plagioclase. Furthermore, there is partial replacement of orthopyroxene by amphibole in the corona, reflecting amphibole superseded orthopyroxene crystallization.

As Fig. 9 illustrates on a 2D surface, the change in mineral compositions are relatively sharp at the very edge of each mineral phase. Minerals do not record gradational intracrystalline zoning. X-ray maps clearly show that olivine and plagioclase have experienced grain resorption during the generation of coronitic layers. It can also be observed that the orthopyroxene layer is not continuous in rimming olivine.

The presence of orthopyroxene rims around olivine reflects introduction of SiO_2 during the generation of this corona layer (Fig. 10A). In effect, the SiO_2 content in orthopyroxene being higher than in all of the other phases makes the distinction, because all the other major cations either decrease (Al and Ca) or increase (Mg and Fe) from plagioclase to olivine (Figs. 9 and 10A,B). Since both anorthite-rich plagioclase and olivine have lower SiO_2 than orthopyroxene, only the breakdown of plagioclase to amphibole would provide the SiO_2 necessary to form orthopyroxene from olivine. If it is the case, the orthopyroxene-forming mechanism needs to be coupled with the one generating amphibole. The requirement of H_2O to form amphibole also indicates involvement of either a water-rich residual melt or a separated fluid phase.

It is difficult to discern whether cumulate olivine and plagioclase grains were in full contact or not before the coronal reaction process began. Furthermore, there is no evidence that the replacement of corona layers resulted from changes in pressure or temperature as amphibole composition is the same in the intercumulus and coronas. However, there is petrographic evidence that this reaction consumes olivine and to a lesser extent plagioclase without changing the composition of reactant plagioclase and olivine (Fig. 10A and B, see also Section 5).

In the Sierra de Valle Fértil we have examined several tens of coronitic gabbroic rocks, from which an essential observation has already been reached, if olivine and plagioclase do not coexist, no coronas are present. Formation of the coronas requires a set of chemical components that exists only where olivine and plagioclase coexist (Figs. 9 and 10). If the two phases are present then

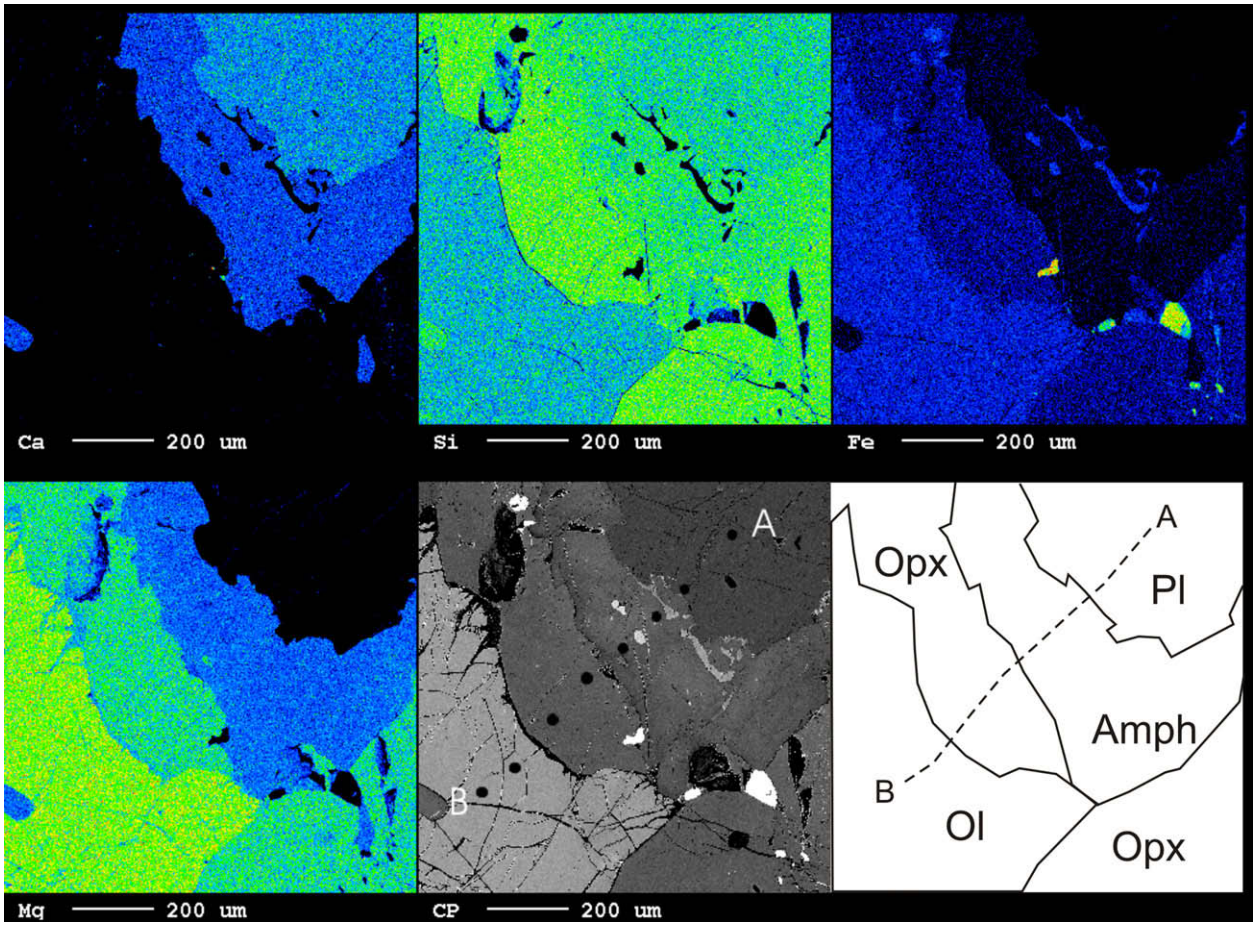

Fig. 9. X-ray compositional maps measured for qualitatively analyzing the 2D distribution of Ca, Si, Fe, and Mg. Black dots on the BSE image (centre of the bottom panels) show the location of the analyzed spots that were then used to construct the Fig. 10. A sketch showing the boundary among mineral phases is drawn on the right side of the bottom panels. This sketch also shows the location of the transverse (A–B) connecting the analyzed spots.

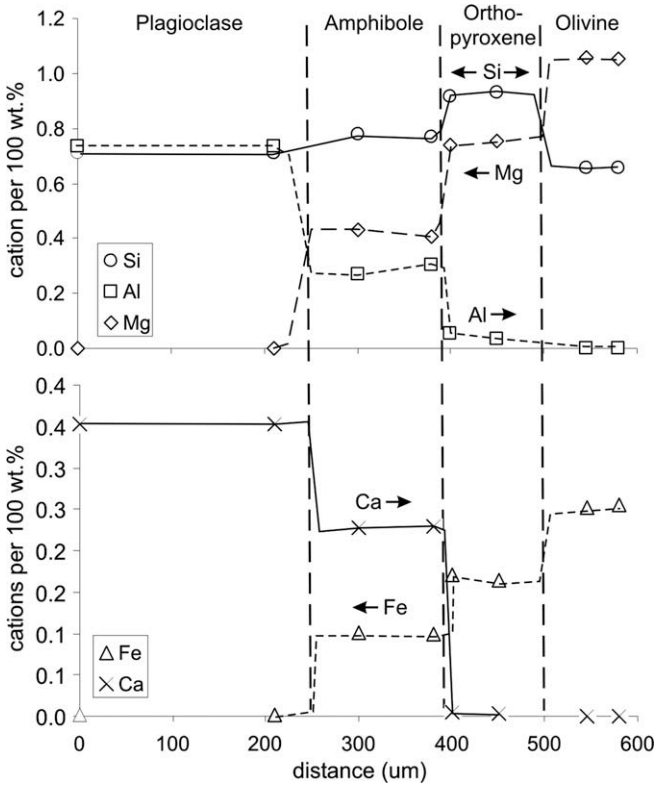

Fig. 10. Compositional profiles show the variation of major elements in mineral phases that are spatially related by a typical corona reaction texture. Small arrow points to the direction to which each cation tends to move by ion–self diffusion. Further details are given in Fig. 9 and text.

the coronas may form at supersolidus or sub-solidus conditions, albeit at very high *T*. If these phases do not coexist, the coronas will not form in either case. One would expect that a sub-solidus solid-state metamorphic mechanism not to be so selective. In this particular case an unrelated metamorphic event post-dating mafic magmatism would have, at least, overprinted the pristine igneous textures. The idea we prefer is that the generation of corona texture found in gabbroic cumulate containing olivine and plagioclase was due to the reaction of the crystallized phases with late-stage magmatic liquids and/or hydrous fluids (e.g. de Haas et al., 2002).

8. Major element fractionation evolution

Specimens taken for whole-rock chemical analyses consist of more than 2 kg of wholly fresh material. After crushing the whole sample, approximately 500 g of homogenous pebble-sized material were pulverized within an agate grinding bowl. The container was always pre-contaminated with the sample about to be pulverized. Major elements were determined by ICPAES at the ACME Laboratories, Vancouver, Canada. Sample VFJA4 was analysed as both known and unknown, and both the known sample and its duplicate datum are reported in Table 5. Trace elements were determined by ICP-MS using a HP4500® housed at the University of Huelva, Spain (see de la Rosa et al., 2001).

Each gabbroic and peridotitic rock has a whole-rock composition that reflects the abundance of each mineral forming the cumulate (Fig. 11A and B). The Mg-number (=Mg# as defined above) of the distinct rock types positively correlates with the composition and proportion of the ferromagnesian phases (Fig. 11A). The Mg# varies from 0.80 in the amphibole pyroxene peridotite to 0.67 in the clinopyroxene amphibole gabbronorite. Whole-rock Mg#s are, however, estimated assuming a Fe_2O_3/FeO of 0.20, because this Fe_2O_3/FeO ratio allows balancing by masses the whole-rock compositions and mineral compositions weighted by their modal proportions. Since the Fe_2O_3/FeO ratio computed by mass balance lies within the range of Fe_2O_3/FeO ratios estimated through oxygen barometry (i.e. reaction (1)), mass balance provides an independent evidence for the conclusion that oxygen fugacity of the mafic magma was similar to, or close above, that of the FMQ buffer (i.e. reaction (2)) at temperature and pressures of crystallization.

In particular, the Mg#s (*ca.* 0.8) of olivine-bearing rocks from the Jaboncillo body are too high to represent any magma observed in the Phanerozoic. Only picrite basalts that have experienced olivine accumulation have these Mg#s (Ramsay et al., 1984). We note the olivine-bearing rocks fall along, or very close to, the tie-line between olivine and plagioclase in the CaO vs. MgO variation diagram. Thus, as inferred from the modal variation among rock types (Fig. 3D), differentiation of the magma between 30 and 9 wt.% MgO may have been solely controlled by separation of olivine from plagioclase (Fig. 11B).

The influence of clinopyroxene and plagioclase crystallization on magma evolution can be seen in the CaO vs. Al_2O_3 diagram (Fig. 11C). Early depletion of CaO with minor variation of Al_2O_3 is better explained by clinopyroxene just preceding plagioclase crystallization. An alternative explanation is to assume that amphibole was an early magmatic phase; however this assumption would contradict petrographic observations. When gabbroic and peridotitic rocks from the Jaboncillo layered body are compared with rocks from the mafic unit from Sierras Valle Fértil and La Huerta (Otamendi et al., 2009), it can be seen that the separation of olivine-rich and plagioclase-rich cumulates does not explain the evolutionary trend found in this mafic unit (Fig. 11B and C). As suggested by the rock modes, the olivine stops crystallizing over a few meters outside the limit of the gabbroic and peridotitic layered body. This observation has also been found in other cumulate bodies from the Sierra Valle Fértil–La Huerta (unpublished data). Therefore, a combination of orthopyroxene and amphibole, which in turn become the most abundant ferromagnesian minerals, take the role of olivine in controlling the differentiation trend of increasing SiO_2 with decreasing MgO (Fig. 11D).

Incompatible oxides (as exemplified by Na_2O) increase with decreasing MgO (Fig. 11E). The behavior of Na_2O is also followed by other oxides such as TiO_2 and K_2O. Whereas K_2O remains too low to stabilize a K-bearing rock-forming mineral (i.e. micas and K-feldspar), the TiO_2 enrichment causes the first ilmenite crystallization accompanying magnetite in the olivine-absent gabbronorites. An increase of TiO_2 content in the magma, rather than a reduction of oxygen fugacity, results in ilmenite crystallization.

9. Trace element chemistry

The trace element patterns normalized to N-MORB for both mafic and ultramafic cumulate rocks show enrichments in lithophile incompatible elements, positive Pb and Sr anomalies, Nb and Ta depletion, and an overall decrease of elemental abundance with increasing mantle compatibility (Fig. 12A). These rocks are characterized by enrichments in LILE and depletions in HFSE relative to the Normal-MORBs composition. Although the trace element patterns are similar to those of plutonic and volcanic rocks in arc settings (e.g. Wilson, 1989), as one would expect for a cumulate the abundance of incompatible trace elements is too low to even be primitive arc magma. Elements with mantle-melting bulk partition coefficients (*D*) higher than Nb are well below MORB composition. By contrast, excluding HFSE (Nb and Ta) elements with $D < Nb$ are similar or above MORB abundances. Notably, the light rare earth (La and Ce), which have abundances from 0.3 to 0.6 times lower

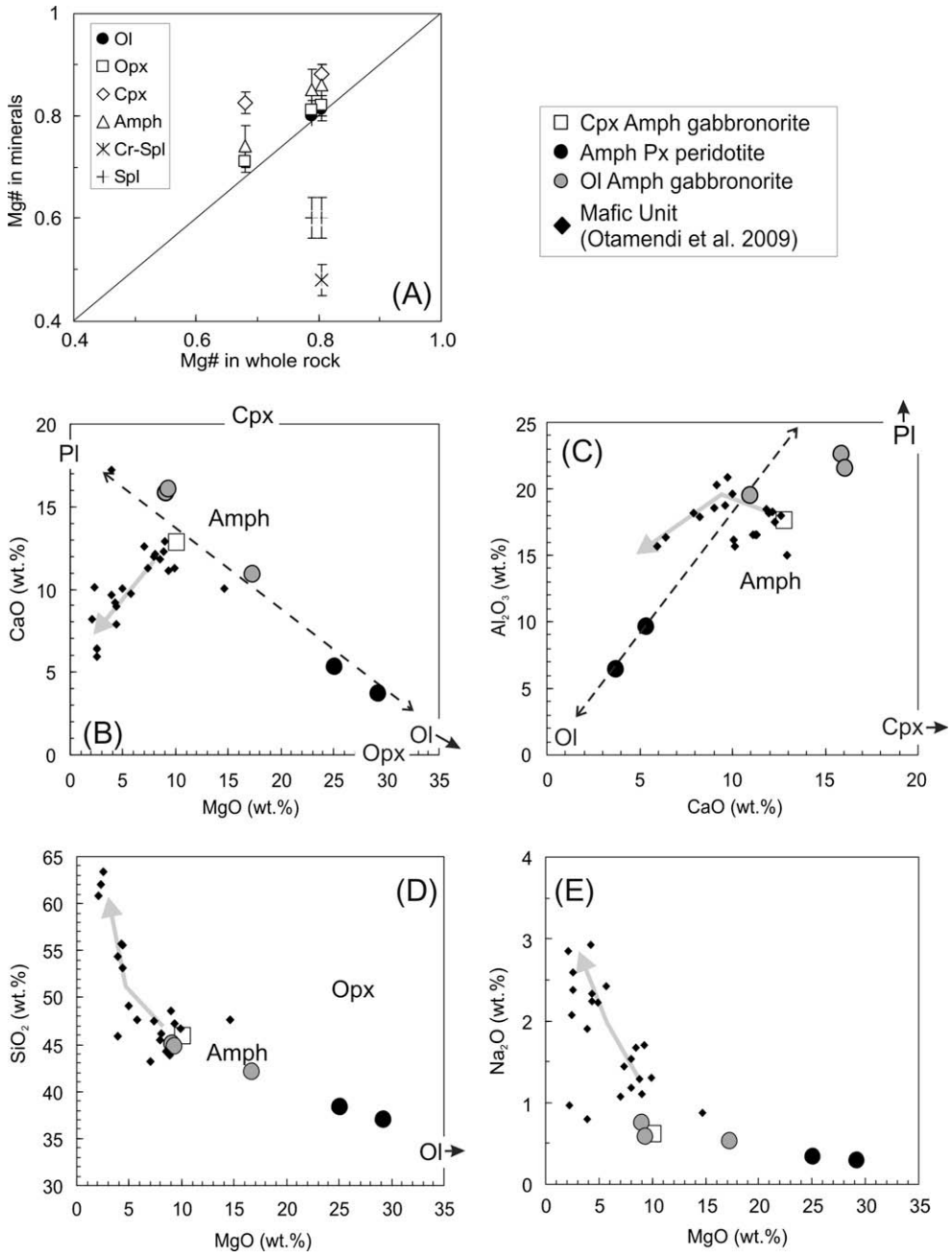

Fig. 11. (A) Mg-number in whole rock vs. Mg-number in minerals for mafic and ultramafic rocks from the Jaboncillo Valley. (B–E) Bivariante plots of the oxides CaO, MgO, Al_2O_3, SiO_2 and Na_2O for mafic and ultramafic rocks from the Jaboncillo Valley and selected rocks in the mafic unit from Sierras Valle Fértil–La Huerta taken after Otamendi et al. (2009). Representative compositions of mineral phases are those presented in Table 1. Double-arrow dashed line connects olivine and plagioclase composition in the CaO vs. MgO and Al_2O_3 vs. CaO bivariante plots. The grey line is arbitrarily drawn to show the chemical trends in the mafic unit from Sierras Valle Fértil–La Huerta.

than those of typical N-MORB, appear below their expected concentrations (Fig. 12A). Furthermore, all cumulate types from the Jaboncillo Valley body show that elements with $D >$ Nb are from 2 to 100 times lower than their concentrations in the best candidate for representing a parental magma composition from Valle Fértil–La Huerta crustal section (i.e. gabbro LHBL22). Mafic and ultramafic cumulate rocks, however, retain a similar trace element signature to the gabbronoritic and gabbroic rocks dominating the mafic unit from Valle Fértil–La Huerta arc crustal section (see Otamendi et al., 2009), so reflecting a genetic relationship among them.

The ultramafic pyroxene amphibole peridotite rocks have chondrite-normalized (REE_N) pattern with higher light-REE than middle- and heavy-REE ($La_N/Gd_N \sim 4.25$ and $La_N/Yb_N \sim 5.6$; Fig. 12B). These rocks show no Eu anomalies and a nearly flat middle- to heavy-REE normalized pattern. The REE pattern with high La_N/Gd_N is difficult to be explained in terms of mineral proportion because peridotite rock type largely consists of olivine (Ol > 40% modal). As discussed below, the most plausible explanation for this discrepancy is that inter-cumulus minerals crystallized in equilibrium with a trapped melt fraction (TMF) containing higher REE concentrations than the parental magma (e.g. Bédard, 1994; Claeson and Meurer, 2004). By contrast, the olivine pyroxene amphibole gabbronorites have also a smooth but less steep REE pattern ($La_N/Gd_N \sim 2$ and $La_N/Yb_N \sim 2.9$; Fig. 12B). The lack of a clear Eu anomaly in all of the olivine-bearing mafic and ultramafic rocks reflects

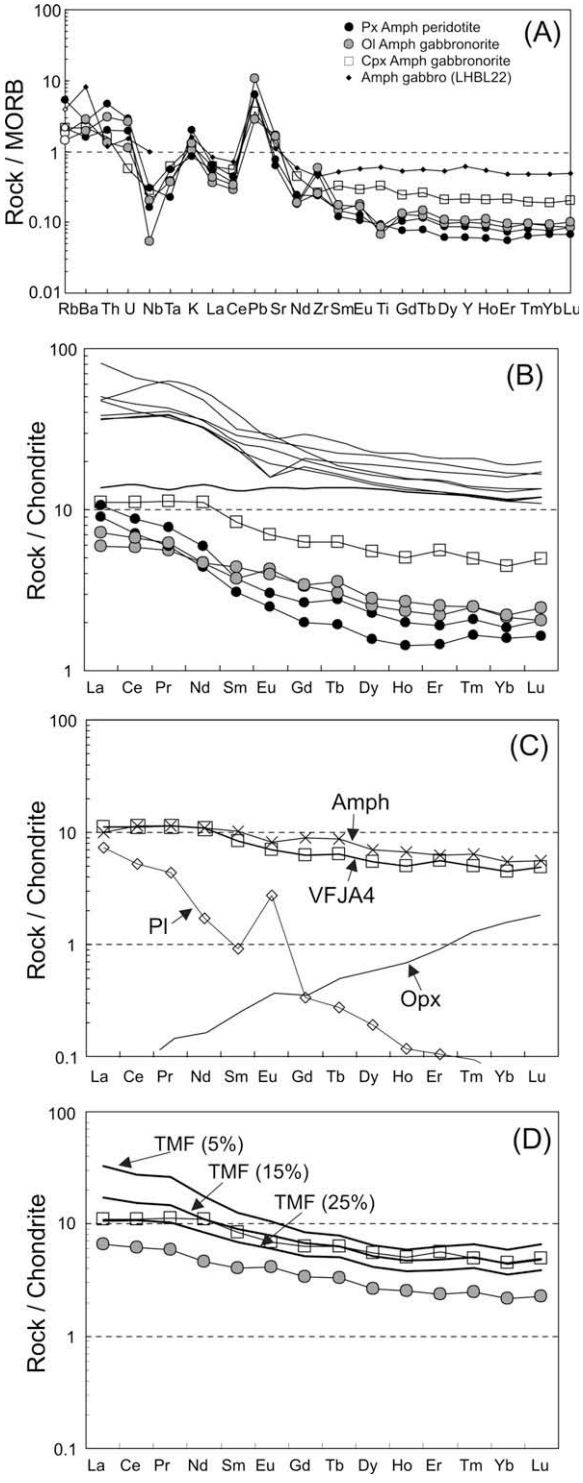

Fig. 12. (A) Trace element composition for mafic and ultramafic rocks from the Jaboncillo Valley, normalized to N-MORB values from Hofmann (1988). (B) Rare earth element abundances for rocks in panel (A) normalized to C1 chondrite from Anders and Grevesse (1989). For comparison it has been also plotted the REE pattern (i.e. thin solid lines) of selected rocks in the mafic unit from Sierras Valle Fértil–La Huerta taken after Otamendi et al. (2009). (C) Chondrite normalized REE patterns calculated for orthopyroxene (Opx), plagioclase (Pl) and amphibole (Amph) from the clinopyroxene amphibole gabbronorite (VFJA4). The REE content of minerals was computed by the equilibrium distribution method at 0% trapped melt fraction (TMF) and following a procedure taken after Bédard (1994). (D) Chondrite normalized patterns showing REE contents of residual melts estimated through element inversions and varying the TMF from 5% to 25%. Details about modeling and assumption are given in the text.

that plagioclase played a subordinate role in partitioning the REE between magma and cumulates assemblages. The pyroxene amphibole gabbronorite (VFJA4) shows higher REE contents than the olivine-bearing rocks, but for elements heavier than Nd, this gabbronorite still have REE concentration 3–4 times below that of the most primitive rock from the mafic unit (Fig. 12A).

The trace element compositions of melt in equilibrium with the evolving cumulate may be estimated using a bulk-rock inversion approach (see Bédard, 1994). The method computes the abundance of trace element in each cumulate phase from the whole-rock composition, mineral modal abundance, and a consistent set of mineral/melt distribution coefficients (Bédard, 1994). The critical assumptions in this model are that all of the mineral in a given cumulate assemblage crystallized from the same melt at the same temperature, and solid–liquid equilibrium prevails; and that the inter-cumulus minerals crystallized from an interstitial trapped melt fraction (TMF) initially in equilibrium with the cumulus minerals (Claeson and Meurer, 2004). The concentration (C) of a trace element i in a multi-phase mineral assemblage obey the mass balance equation:

$$C^i_{\text{rock}} = \left(x_1 C^i_1 + x_2 C^i_2 + \cdots + x_n C^i_n + x_{\text{melt}} C^i_{\text{melt}}\right) \quad (3)$$

which equates the whole-rock abundance (C^i_{rock}) of the trace element (i) to the total sum of concentration in minerals (C^i_1 stands for concentration of trace i in mineral 1) times the mass fraction of each phase in the mineral assemblage (x_1 is mass fraction of mineral 1). After introducing mineral/liquid partition coefficients and re-arranging, the concentration of element i in mineral 1 can be obtained from the equation:

$$C^i_1 = C^i_{\text{rock}} \Big/ \left(x_1 + x_2 \text{Kd}^i_2 \Big/ \text{Kd}^i_1 + \cdots + x_n Kd^i_n \Big/ \text{Kd}^i_1 + x_{\text{melt}} / \text{Kd}^i_1\right) \quad (4)$$

With Eq. (4) we compute the REE concentration in plagioclase, orthopyroxene and amphibole in an average composition of two olivine amphibole gabbronorites (i.e. VFJA58 and VFJA64 in Table 5). The partition coefficients (Kd^i_n) of REE between minerals and melt are those compiled by Bédard (1994) and Claeson and Meurer (2004). The weight fraction of minerals in the average (x_n) is estimated by mass balance between whole-rock and mineral composition using least-square multiple-regressions. As estimated by mass balance, the weight fraction of minerals in the model olivine amphibole gabbronorite is: 5% olivine, 13% of orthopyroxene, 40% of plagioclase, 36% of amphibole, and 7% of ulvospinel (Al-spinel plus magnetite). The computed mineral mass fraction yields higher plagioclase proportions than in the olivine amphibole gabbronorites (see Table 5). However, the whole-rock CaO content (~16 wt.%) is better accounted for the plagioclase fraction determined by mass balance in these rocks.

Initially, the trapped melt fraction (i.e. x_{melt} in Eq. (4)) was assumed to be zero. Numerical modelling gives REE patterns in plagioclase, orthopyroxene and amphibole closely matching published values (Fig. 12C). A weak aspect of this study is that we have not measured trace element concentration in mineral to test model and measured concentration (e.g. Bédard, 1994; Meurer and Claeson, 2002; Claeson and Meurer, 2004). The main result from modelling is that amphibole incorporates much higher amounts of REE than all of the other coexisting phases, and this conclusion would not be significantly challenged by performing trace *in situ* mineral analyses. Because amphibole is a late crystallizing phase, the REE signature of model melts during cumulate formation depends upon whether the stability field of amphibole was already reached by the evolving magmatic system (Claeson and Meurer, 2004). A conclusion that is also valid for most incompatible trace elements.

As shown by Claeson and Meurer (2004) and here suggested by petrography, amphibole is the product of a late magmatic reaction between plagioclase, olivine and trapped melt. Thus, in order to test how amphibole crystallization depletes the trace element abundance of the trapped melt fraction, we modelled the composition of melts at 0.05, 0.15 and 0.25 fractions, and under the assumption that all the late-magmatic trapped melt crystallized as interstitial amphibole (Fig. 12D). Models indicate that both the enrichment (ΣREE) and steepness (La/Yb) of the REE pattern increase with decreasing melt fractions and amphibole fraction in the solid assemblage. It follows that the content of incompatible trace elements in the trapped melt increases as the melt fraction decrease, but is at some extent lowered by amphibole crystallization. The range of modelled liquid compositions overlaps with the REE content of the clinopyroxene amphibole gabbronorite (VFJA4) residing at the top of the Jaboncillo Valley body (Fig. 12D), suggesting that internal differentiation of the magma bodies occurred when residual melts were drained from highly crystallized olivine + spinel + pyroxene + plagioclase crystal mush and while amphibole was beginning to be stable.

Although here we are not able to provide quantitative proofs, a similar magmatic process but operating within the olivine-absent clinopyroxene amphibole gabbronorites would explain the REE contents of most common gabbronorites from the Sierra Valle Fértil–La Huerta (see Fig. 12C). Nevertheless, the composition of the parental magma feeding the mafic and ultramafic layered body cannot be retrieved from trace element systematics.

10. Constraints on parental melt composition for the Jaboncillo Valley body

Cumulate rocks do not show the magma composition in any simple fashion (e.g. Cox et al., 1979). Thus, several lines of evidence are usually used to constraint the most likely composition of the magma that fed layered cumulate sequences (see DeBari, 1997).

Roeder and Emslie (1970) were first to demonstrate that the exchange coefficient $\left[K_D^{Mg-Fe}\right]$ olivine–liquid is essentially independent of temperature and small variations in liquid composition. It has been shown recently that the Fe–Mg partition coefficient between olivine and liquid is around 0.32 (e.g. Pichavant and Macdonald, 2007). Thus, olivine (Fo = 0.81–0.82) crystallized from magmas with Mg-number of around 0.59–0.61. Hence, even the evolved olivine-absent clinopyroxene amphibole gabbronorite (VFJA4) having Mg-number of 0.67 does not reflect the parental magma composition.

Projecting rocks and mineral compositions in the MgO vs. FeO* co-variation diagram reveals that olivine-bearing rocks are perfect mixtures of olivine and plagioclase (Fig. 13A). Moreover, as suggested above, the reaction among these minerals and late-magmatic melts resulted in orthopyroxene and amphibole. Thus, the simple subtraction of a combination of olivine plus plagioclase to the clinopyroxene amphibole gabbronorite (VFJA4) would move the composition of the gabbronorite to the theoretical composition of the melt with Mg# ~ 0.6 (Fig. 13A). Within this simple chemical system, gabbronorite (VFJA4) is regarded as a mixture of cumulate minerals and true parental melt, the problem is to solve what point on the olivine–plagioclase tie-line better represents the cumulate minerals in the gabbronorite. Although the gabbronorite has an olivine-absent igneous assemblage, early crystallized olivine might have been totally consumed by the orthopyroxene- and amphibole-forming reactions. So, considering a cumulate assemblage controlled by olivine and plagioclase that varied over the full range of olivine/plagioclase ratios found within the Jaboncillo body, it is possible to deduce the MgO and FeO* content of the parental magma (Fig. 13A). The latter diagram illustrates that removing a cumulate composition within the range olivine–plagioclase assemblages to gabbronorite VFJA4 intersect the theoretical melt with Mg = 0.6 at a range of MgO (7.2–9.2 wt.%) and FeO (8.6–11 wt.%) contents.

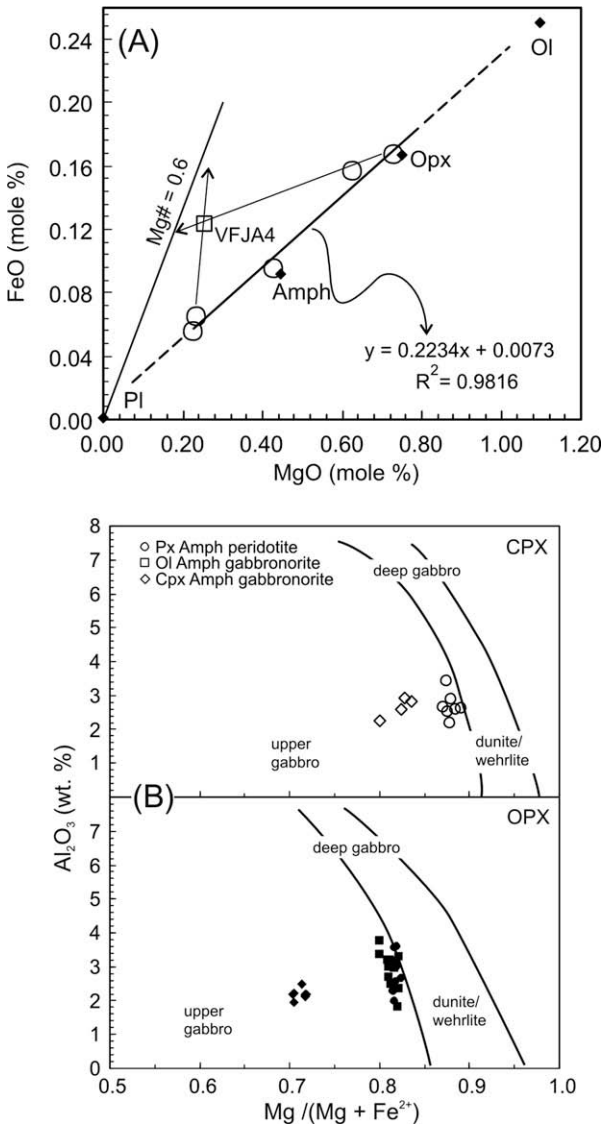

Fig. 13. (A) MgO vs. FeO diagram on a molar basis for whole-rock and minerals from mafic and ultramafic layered rocks. It is also shown a least-square fitted regression line that was computed only using olivine-bearing rocks. Note that if the regression line is extrapolated, it joins olivine and plagioclase compositions. Two arrows show the predicted path of derivative melts as it is extracted either olivine-dominated or plagioclase-dominated assemblages from a magma represented by the clinopyroxene amphibole gabbronorite (VFJA4). In the text we argument that the most likely MgO and FeO composition of the parental melt is obtained from the intersection between the derivative melt and a theoretical melt having Mg-number = 0.6. (B) Plot of Al_2O_3 wt.% vs. Mg-number in clinopyroxene (upper panel) and orthopyroxene (lower panel) from Jaboncillo Valley rocks. The field of progressively higher Al in the pyroxenes with differentiation (e.g. decreasing Mg-number) from ultramafic and mafic rocks in deep-seated crustal levels is after DeBari and Coleman (1989). The Al and Mg-number of pyroxenes in upper crustal gabbro is also from these authors.

By implication, considering that the Fe_2O_3/FeO ratio was around 0.2, the ferric oxide concentration was between 1.7 and 2.2 wt.%. Moreover, if the parental melt had MgO slightly higher than 8 wt.%, the MgO vs. SiO_2 compositional trend indicates that the SiO_2 abundance of the parental magma was around or close below 48 wt.% (Fig. 11D). Although this SiO_2 content clearly implies for a mafic magma, the range of Mg-numbers estimated for the parental magma is too low to be in equilibrium with a peridotitic mantle

rock, reflecting that primary magmas parental to Jaboncillo Valley rocks experienced igneous differentiation while moving through the uppermost mantle or the lowermost crust. Following the same reasoning as used for SiO_2, and using the computed range of MgO concentration, the concentration of CaO in the parental magma is estimated to be around 13 wt.% (Fig. 11B).

Major element co-variation chemical trends and Al_2O_3 concentration in pyroxenes provide the strongest evidence for inferring the Al_2O_3 content of the parental magma to the Jaboncillo Valley layered rocks. Excluding olivine-dominated peridotitic cumulates, the chemical trend displayed by the Al_2O_3 variation against MgO, SiO_2 and CaO (Fig. 11C) suggest that the Al_2O_3 should have been higher than 15 wt.%. Additionally, the projection of Al_2O_3 in clinopyroxene and orthopyroxene vs. Mg-numbers (Fig. 13B) does not display the typical trend of increasing Al with decreasing Mg-numbers that is taken to reflect the increment of Al_2O_3 in the evolving mafic magmas (e.g. DeBari and Coleman, 1989). Instead, the two pyroxenes in the olivine-absent gabbronorite (VFJA4) have Al_2O_3 contents overlapping those of pyroxenes in the olivine-present mafic–ultramafic layered rocks (Fig. 13B). And, as expected, the pyroxene Mg-numbers are lower in the former than in the latter rock types. Since the solubility of Al in pyroxenes is a strong function of pressures (Gasparik, 1984), both the almost constant Al_2O_3 abundance in clinopyroxene and orthopyroxene (2–4 wt.%), and the trend of slight decrease of Al with decreasing Mg-numbers in pyroxenes may simply reflect that the studied rocks crystallized at moderate pressures (e.g. DeBari and Coleman, 1989; Jagoutz et al., 2007). At Jaboncillo Valley, the formation of mafic–ultramafic layered cumulates did not lead to significant Al_2O_3 increase, indicating that plagioclase appeared as liquidus phase close after olivine (Crawford et al., 1987; DeBari, 1997), and also suggesting that the parental magma had Al_2O_3 contents higher than those characteristics of high-Mg low-Al basalts.

It is now widely accepted that the variation from parental high-magnesium to derivative high-alumina magmas is intrinsic to arc magmatism evolving at depths of the mantle–crust boundary (Crawford et al., 1987; Gust and Perfit, 1987; DeBari, 1997), making that alumina concentration to be one of the diagnostic parameters in determining how much a primitive magma has evolved. Although the Al_2O_3 content of the parental magma to Jaboncillo Valley rocks cannot be estimated with acceptable accuracy, there are however enough observations to conclude that this parental magma was in terms of Al_2O_3 abundance transitional between high-Mg and high-Al basalts. Importantly, at least in the Famatinian case, the transition from high-magnesium to high-alumina magmas should have begun at pressures higher than 7 kbar.

Amphibole crystallizes throughout the igneous sequence, and forms both magmatic inter-cumulus grains and late- to post-cumulus reaction rims. Oikocrysts and poikilitic crystals of amphiboles are also widespread in the olivine-bearing rocks. At the estimated crystallization pressures (5–7 kbar), magmatic H_2O content is the critical variable in determining the amphibole-in temperature for a mafic magma (Foden and Green, 1992). Further evidence for a mafic hydrous magma is suggested by the high anorthite content in plagioclase (e.g. Arculus and Wills, 1980) and the high wollastonite content in clinopyroxene (e.g. Gaetani et al., 1993). However, as suggested by the high temperature (1200 °C) of olivine and pyroxenes crystallization (Table 2), the initial water content of the mafic primitive magma should have been below 2 wt.% (e.g. Pichavant and Macdonald, 2007). The widespread presence of amphibole in the mafic and ultramafic rocks from the Jaboncillo Valley indicates that magmatic H_2O content of the melt was, at some point of the crystallization, between 3 and 5 wt.% (Foden and Green, 1992). The initial water content of the parental magma was lower than these values, because early crystallization of anhydrous minerals leads to increase the water proportion of the mafic magma, and in turn results in enlargement of the amphibole stability field in a basaltic system (Helz, 1973). However, simple mass balance calculation show that the original water content must be between 1 and 2 wt.% to rise higher than 3 wt.% at around 50% of magma crystallization.

11. Geological implications for the Early Ordovician Famatinian–Puna paleo-arc

Previous arguments give strong evidence for the fact that large amounts of primitive magmas ascend through the lower crust and emplaced at relatively high (20–25 km) paleo-depths in the Famatinian–Puna magmatic arc (see also Otamendi et al., 2009). This observation is important because several other studies have found large volume of plutonic and volcanic mafic sequences all over the Early Ordovician paleo-arc (Mannhein and Miller, 1996; Toselli et al., 1996; Vujovich et al., 1996; Coira et al., 1999, 2009; Kleine et al., 2004; and references therein). Notably, primitive mafic magmatism not only was dominating the crust up to relatively upper levels (*ca.* 20 km depths) but also was fluxing throughout the entire upper crust and feeding volcanoes all along the Early Ordovician magmatic arc. These findings make very unlikely a geodynamic model that regard the Famatinian–Puna magmatic arc as an Andean-type arc (e.g. Lucassen and Franz, 2005).

Evolved (intermediate to silicic) crust should act as a density filter. The possibility that a mafic magma reaches the Earth's surface depends on: (1) crustal-scale structural features, (2) the thickness and composition of the rock pile residing above the seismological Moho, and (3) the proportion of water dissolved in the mafic magma (Herzberg et al., 1983; Tassara, 2006). As evolved arc crust thickens, the buoyant force driving the rise of mafic magmas becomes neutral at progressively deeper depths (Tassara, 2006). The observation that mafic plutonic and volcanic rocks dominate island arc; whereas, on the other extreme, andesite to rhyolite predominate in continental arc build upon thick continental crust (e.g. Puna – Altiplano case), is simply explained by this physical control. From it follows that, the common igneous differentiation trend leading to progressively more buoyant magmas is the natural reason that explains why the crust would tend to be lithologically stratified as the arc becomes more mature (Tatsumi et al., 2008). Thus, from simply and well-known physical and chemical arguments, we cannot support the idea that the ancient Famatinian–Puna arc resembles in several aspects the present-day South American Andes. It should however be noted that we are not claiming the Famatinian–Puna paleo-arc was an intra-oceanic Mariana-type arc.

12. Conclusions

The effect that has amphibole crystallization as both magmatic inter-cumulus grains and late- to post-cumulus reaction rims is one of the most relevant conclusions of this study. Because, if amphibole crystallizes at a late magmatic stage, it would drastically raise the bulk distribution coefficients of the magmatic assemblage, leading to the retention of trace elements, which would otherwise behave strongly incompatible with the mafic and ultramafic cumulate assemblage (e.g. Claeson and Meurer, 2004). Since this study shows that amphibole-rich cumulates are widespread at lower crustal levels of magmatic arcs, the amphibole cumulates would exert an important control on the water and incompatible trace element budget of arc-related magmatism (Meurer and Claeson, 2002; Davidson et al., 2007).

In virtually all of the volcanic arcs, hydrous primitive magmas pond and emplace at relatively deep levels to form mafic–ultramafic cumulate sequences (DeBari, 1997). Hence, another goal of

this study is to demonstrate that in some cases the cumulate layered sequences are made up by magmas that either have already left behind an olivine–pyroxene cumulate or derived after partially melting source dominated by the olivine–pyroxene assemblage. In fact, if the seismic arc Moho is regarded as the level separating plagioclase-bearing from plagioclase-free igneous rocks, these petrological processes largely happen within the lower crust.

Acknowledgment

This research is supported by FONCyT – Argentina Grants PICTR20298/04 and PICT01904/07. Field work was partly funded by grants of the Universidad Nacional de Río Cuarto, Argentina. We acknowledge to Professor A. Patiño Douce and an anonymous journal reviewer for providing extremely constructive criticisms that greatly improved the manuscript in both clarity and scientific content. We are grateful to Professor George Bergantz who provided final reading that corrected writing style and strengthened arguments.

References

Aceñolaza, F.G., Miller, H., Toselli, A.J., 2000. The Pampean and Famatinian cycles – superposed orogenic events in the West Gondwana. Sonderheft ZAG SH 1, 337–344.

Anders, E., Grevesse, N., 1989. Abundances of the elements–meteoritic and solar. Geochimica et Cosmochimica Acta 53, 197–214.

Arculus, R.J., Johnson, R.W., 1978. Criticism of generalized models for the magmatic evolution of arc–trench systems. Earth and Planetary Science Letters 39, 118–126.

Arculus, R.J., Wills, K.J.A., 1980. The petrology of plutonic blocks and inclusions from the Lesser Antilles Island Arc. Journal of Petrology 21, 743–799.

Astini, R.A., Dávila, F.M., 2004. Ordovician back arc foreland and Ocloyic thrust belt development on the western Gondwana margin as a response to Precordillera terrane accretion. Tectonics 23, TC4008. doi:10.1029/2003TC001620.

Baker, D.R., Eggler, D.H., 1983. Fractionation paths of Atka (Aleutians) high-alumina basalts: constraints from phase relations. Journal of Volcanology and Geothermal Research 18, 387–404.

Baldo, E.J., Murra, J., Casquet, C., Saavedra, J., Galindo, C., 1999. Gabros coroníticos de la Sierra de Valle Fértil. Química mineral y condiciones *P–T*. Sierras Pampeanas Occidentales (Argentina). Boletín de la Sociedad Española de Mineralogía 22A, 17–19.

Ballhaus, C., Berry, R.F., Green, D.H., 1991. High pressure experimental calibration of the olivine–orthopyroxene-spinel oxygen geobarometer: implications for the oxidation state of the upper mantle. Contributions to Mineralogy and Petrology 107, 27–40.

Beard, J.S., 1986. Characteristic mineralogy of arc-related cumulate gabbros: implications for the tectonic setting of gabbroic plutons and for andesite genesis. Geology 14, 848–851.

Beard, J.S., Borgia, A., 1989. Temporal variation of mineralogy and petrology in cognate gabbroic enclaves at Arenal volcano, Costa Rica. Contributions to Mineralogy and Petrology 103, 110–122.

Bédard, J.H., 1994. A procedure for calculating the equilibrium distributions of trace elements among minerals of cumulate rocks, and the concentration of trace elements in the coexisting liquids. Chemical Geology 118, 143–153.

Berman, R.G., 1988. Internally-consistent thermodynamic data for minerals in the system Na_2O–K_2O–CaO–MgO–FeO–Fe_2O_3–Al_2O_3–SiO_2–TiO_2–H_2O–CO_2. Journal of Petrology 29, 445–522.

Brey, G.P., Köhler, T., 1990. Geothermobarometry in four-phase lherzolites II. New thermobarometers, and practical assessment of existing thermobarometers. Journal of Petrology 31, 1353–1378.

Caminos, R., 1979. Sierras Pampeanas Noroccidentales. Salta, Tucumán, Catamarca, La Rioja y San Juan. In: Leanza, E.F. (Ed.), II Simposio de Geología Regional Argentina. Academia Nacional de Ciencias de Córdoba, pp. 225–291.

Claeson, D.T., 1998. Coronas, reaction rims, symplectites and emplacement depth of the Rymmen gabbro, Transscandinavian Igneous Belt, southern Sweden. Mineralogical Magazine 62, 743–757.

Claeson, D.T., Meurer, W.P., 2004. Fractional crystallization of hydrous basaltic "arc-type" magmas and the formation of amphibole-bearing gabbroic cumulates. Contributions to Mineralogy and Petrology 147, 288–304.

Coira, B., Pérez, B., Flores, P., Kay, S.M., Woll, B., Hanning, M., 1999. Magmatic sources and tectonic setting of Gondwana margin Ordovician magmas, northern Puna of Argentina and Chile. In: Ramos, V., Keppie, J. (Eds.), Laurentia-Gondwana connections before Pangea, Geological Society of America Special Paper 336, pp. 145–170.

Coira, B., Koukharsky, M., Ribeiro Guevara, S., Cisterna, C.E., 2009. Puna (Argentina) and northern Chile Ordovician basic magmatism: a contribution to the tectonic setting. Journal of South American Earth Sciences 27, 24–35.

Conrad, W.K., Kay, R.W., 1984. Ultramafic and mafic inclusions from Adak Island: crystallization history and implications for the nature of primary magmas and crustal evolution in the Aleutian arc. Journal of Petrology 25, 88–125.

Cox, K.G., Bell, J.D., Pankhurst, R.J., 1979. The Interpretation of the Igneous Rocks. George Allen & Unwin.

Crawford, A.J., Falloon, T.J., Eggins, S., 1987. The origin of island arc high-alumina basalts. Contributions to Mineralogy and Petrology 97, 417–430.

Davidson, J., Turner, S., Handley, H., Macpherson, C., Dosseto, A., 2007. Amphibole "sponge" in arc crust? Geology 35, 787–790.

de Haas, G.-J.L., Nijland, T.G., Valbracht, P.J., Maijer, C., Verschure, R., Andersen, T., 2002. Magmatic versus metamorphic origin of olivine–plagioclase coronas. Contributions to Mineralogy and Petrology 143, 537–550.

de la Rosa, J.D., Chacón, H., Sánchez de la Campa, A., Carrasco, R., Nieto, J.M., 2001. Metodología y análisis de elementos trazas-REE mediante ICP-MS del standard SARM 1 (granito) y SARM 4 (norita). In: Lago, M., Arranz, E., Galé, C. (Eds.), Libro de Actas del III Congreso Ibérico de Geoquímica. Zaragoza, España, pp. 435–438.

DeBari, S., 1994. Petrogenesis of the Fiambalá gabbroic intrusion, Northwestern Argentina, a deep crustal syntectonic pluton in a continental magmatic arc. Journal of Petrology 35, 679–713.

DeBari, S., 1997. Evolution of magmas in continental and oceanic arcs: the role of the lower crust. Canadian Mineralogist 35, 501–519.

DeBari, S., Coleman, R.G., 1989. Examination of the deep levels of an island arc: evidence from the Tosina ultramafic–mafic assemblage, Tosina, Alaska. Journal of Geophysical Research 94, 4373–4391.

DeBari, S., Kay, S.M., Kay, R.W., 1987. Ultramafic xenoliths from Adagdak Volcano, Adak, Aleutian Islands, Alaska: deformed igneous cumulates from the Moho of an island arc. Journal of Geology 95, 329–341.

Foden, J.D., Green, D.H., 1992. Possible role of amphibole in the origin of andesite: some experimental and natural evidence. Contributions to Mineralogy and Petrology 109, 479–493.

Gaetani, G.A., Grove, T.L., Bryan, W.B., 1993. The influence of water on the petrogenesis of subduction-related igneous rocks. Nature 365, 332–334.

Gasparik, T., 1984. Two-pyroxene thermobarometry with new experimental data in the system CaO–MgO–Al_2O_3–SiO_2. Contributions to Mineralogy and Petrology 87, 87–97.

Gust, D.A., Perfit, M.R., 1987. Phase relations of a high-Mg basalt from the Aleutian Island Arc: Implications for primary island arc basalts and high-Al basalts. Contributions to Mineralogy and Petrology 97, 7–18.

Helz, R.T., 1973. Phase relations of basalts in their melting range at P_{H20} = 5 kb as a function of oxygen Fugacity. Part I. Mafic Phases. Journal of Petrology 14, 249–302.

Herzberg, C.T., Fyfe, W.S., Carr, M.J., 1983. Density constraints on the formation of the continental Moho and crust. Contributions to Mineralogy and Petrology 84, 1–5.

Hofmann, A.W., 1988. Chemical differentiation of the Earth: relationship between mantle, continental crust and oceanic crust. Earth and Planetary Science Letters 90, 297–314.

Holland, T., Blundy, J., 1994. Non-ideal interactions in calcic amphiboles and their bearing on amphibole–plagioclase thermometry. Contributions to Mineralogy and Petrology 116, 433–447.

Holloway, J.R., Burnham, C.W., 1972. Melting relations of basalt with equilibrium water pressure less than total pressure. Journal of Petrology 13, 1–29.

Jagoutz, O., Müntener, O., Ulmer, P., Pettke, T., Burg, J., Dawood, H., Hussain, S., 2007. Petrology and mineral chemistry of lower crustal intrusions: the Chilas Complex, Kohistan (NW Pakistan). Journal of Petrology 48, 1895–1953.

Johnson, C.D., Carlson, W.D., 1990. The origin of olivine–plagioclase coronas in metagabbros from the Adirondack Mountains, New York. Journal of Metamorphic Geology 8, 697–717.

Johnson, M.C., Rutherford, M.J., 1989. Experimental calibration of the Al-in-hornblende geobarometer with application to Long Valley caldera (California) volcanic rocks. Geology 17, 837–841.

Kay, S.M., Kay, R.W., 1985. Role of crystal cumulates and the oceanic crust in the formation of the lower crust of the Aleutian arc. Geology 13, 461–464.

Kleine, T., Mezger, K., Zimmermann, U., Münker, C., Bahlburg, H., 2004. Crustal evolution along the Early Ordovician Proto-Andean margin of Gondwana: trace element and isotope evidence from the complejo igneo Pocitos (Northwestern Argentina). Journal of Geology 112, 503–520.

Kress, V.C., Carmichael, I.S.E., 1991. The compressibility of silicate liquids containing Fe_2O_3 and the effect of composition, temperature, oxygen fugacity and pressure on their redox states. Contributions to Mineralogy and Petrology 108, 82–93.

Kretz, R., 1983. Symbols for rock-forming minerals. American Mineralogist 68, 277–279.

Le Maitre, R.W., 1989. A Classification of Igneous Rocks and Glossary of Terms. Blackwell, Oxford. pp. 1–193.

Leake, B., Woolley, A., Arps, C., Birch, W., Gilbert, M., Grice, J., Hawthorne, F., Kato, A., Kisch, H., Krivovichev, V., Linthout, K., Laird, J., Mandarino, J., Maresch, W., Nickel, E., Rock, N., Schumacher, J., Smith, D., Stephenson, N., Ungaretti, L., Whittaker, E., Youzhi, G., 1997. Nomenclature of amphiboles: report of the subcommittee on amphiboles of the international mineralogical association, commission on new minerals and mineral names.. American Mineralogist 82, 1019–1037.

Lucassen, F., Franz, G., 2005. The early Palaeozoic Orogen in the Central Andes: a non-collisional orogen comparable to the Cenozoic high plateau? In: Vaughan, A., Leat P., Pankhurst, R., (Eds.), Terrane Processes at the

Margins of Gondwana, Geological Society London Special Publication 246, pp. 257–373.
Mannhein, R., Miller, H., 1996. Las rocas volcánicas y subvolcánicas eopaleozoicas del Sistema de Famatina. In: Aceñolaza, F.G., Miller, H., Toselli, A. (Eds.), Geología del Sistema de Famatina. Münchner Geologische Hefte A19. Münchnen, pp. 159–186.
Meurer, W.P., Claeson, D.T., 2002. Evolution of crystallizing interstitial liquid in an arc-related cumulate determined by LA ICP-MS mapping of a large amphibole oikocryst. Journal of Petrology 43, 607–629.
Mirré, J.C., 1976. Descripción Geológica de la Hoja 19e, Valle Fértil, Provincias de San Juan y La Rioja. Servicio Geológico Nacional, Boletín No. 147, Buenos Aires, pp. 1–70.
Müntener, O., Kelemen, P.B., Grove, T.L., 2001. The role of H_2O during crystallization of primitive arc magmas under uppermost mantle conditions and genesis of igneous pyroxenites: an experimental study. Contributions to Mineralogy and Petrology 141, 643–658.
O'Neill, H.StC., Wall, V.J., 1987. The olivine–orthopyroxene-spinel oxygen geobarometer, the nickel precipitation curve, and the oxygen fugacity of the Earth's upper mantle. Journal of Petrology 28, 1169–1191.
Otamendi, J.E., Tibaldi, A.M., Vujovich, G.I., Viñao, G.A., 2008. Metamorphic evolution of migmatites from the deep Famatinian arc crust exposed in Sierras Valle Fértil–La Huerta, San Juan, Argentina. Journal of South American Earth Sciences 25, 313–335.
Otamendi, J.E., Vujovich, G.I., de la Rosa, J.D., Tibaldi, A.M., Castro, A., Martino, R.D., 2009. Geology and petrology of a deep crustal zone from the Famatinian paleo-arc, Sierras Valle Fértil–La Huerta, San Juan, Argentina. Journal of South American Earth Sciences 27, 258–279.
Pankhurst, R.J., Rapela, C.W., Saavedra, J., Baldo, E., Dahlquist, J., Pascua, I., Fanning, C.M., 1998. The Famatinian magmatic arc in the central Sierras Pampeanas: an Early to Mid-Ordovician continental arc on the Gondwana margin. In: Pankhurst, R.J. Rapela, C.W. (Eds.), The Proto-Andean Margin of Gondwana, Geological Society London Special Publication 142, pp. 343–368.
Pankhurst, R.J., Rapela, C.W., Fanning, C.M., 2000. Age and origin of coeval TTG, I- and S-type granites in the Famatinian belt of NW Argentina. Transactions of the Royal Society of Edinburgh: Earth Sciences 91, 151–168.
Perfit, M.R., Gust, D.A., Bence, A.E., Arculus, R.J., Taylor, S.R., 1980. Chemical characteristics of island arc basalts: implications for mantle sources. Chemical Geology 30, 227–256.
Pichavant, M., Macdonald, R., 2007. Crystallization of primitive basaltic magmas at crustal pressures and genesis of the calc-alkaline igneous suite: experimental evidence from St Vincent, Lesser Antilles arc. Contributions to Mineralogy and Petrology 154, 535–558.
Ramsay, W.R.H., Crawford, A.J., Foden, J.D., 1984. Field setting, mineralogy, chemistry, and genesis of arc picrites, New Georgia, Solomon Islands. Contributions to Mineralogy and Petrology 88, 386–402.
Roeder, P.L., Emslie, L.F., 1970. Olivine–liquid equilibrium. Contributions to Mineralogy and Petrology 29, 275–289.
Sack, R.O., Carmichael, I.S.E., Rivers, M.L., Ghiorso, M.S., 1980. The ferric–ferrous equilibria in natural silicate liquids at 1 bar. Contributions to Mineralogy and Petrology 75, 369–376.
Schmidt, M., 1992. Amphibole composition in tonalite as a function of pressure: an experimental calibration of the Al-in-hornblende barometer. Contributions to Mineralogy and Petrology 110, 421–423.
Sisson, T.W., Grove, T.L., 1993. Experimental investigations of the role of H_2O in calc-alkaline differentiation and subduction zone magmatism. Contributions to Mineralogy and Petrology 113, 143–166.
Snyder, D., Carmichael, I.S.E., Wiebe, R.A., 1993. Experimental study of liquid evolution in an Fe-rich, layered mafic intrusion: constraints of Fe–Ti oxide precipitation on the T–fO_2 and T–ρ paths of tholeiitic magmas. Contributions to Mineralogy and Petrology 113, 73–86.
Spandler, C.J., Arculus, R., Eggins, S.M., Mavrogenes, J.A., Price, R.C., Reay, A.J., 2003. Petrogenesis of the Greenhills Complex, Southland, New Zeland: magmatic differentiation and cumulate formation at the roots of a Permian island-arc volcano. Contributions to Mineralogy and Petrology 144, 703–721.
Tassara, A., 2006. Factors controlling the crustal density structure underneath active continental margins with implications for their evolution. Geochemistry Geophysics Geosystems 7, Q01001. doi:10.1029/2005GC001040.
Tatsumi, Y., Shukuno, H., Tani, K., Takahashi, N., Kodaira, S., Kogiso, T., 2008. Structure and growth of the Izu-Bonin-Mariana arc crust: 2. Role of crust-mantle transformation and the transparent Moho in arc crust evolution. Journal of Geophysical Research 113, B02203. doi:10.1029/2007JB005121.
Toselli, A.J., Durand, F.R., Rossi de Toselli, J.N., Saavedra, J., 1996. Esquema de evolución geotectónica y magmática Eopaleozoica del sistema de Famatina y sectores de Sierras Pampeanas. In: Actas XIII Congreso Geológico Argentino y III Congreso de Exploración de Hidrocarburos 5, pp. 443–462.
Vujovich, G.I., Ramos, V. A., 1999. Mapa geotectónico de la República Argentina (1:2.500.000), Subsecretaría de Minería de la Nación, Buenos Aires, Servicio Geológico Minero Argentino.
Vujovich, G.I., Godeas, M., Marín, G., Pezzutti, N., 1996. El complejo magmático de la Sierra de La Huerta, provincia de San Juan. In: Actas XIII Congreso Geológico Argentino y III Congreso de Exploración de Hidrocarburos 3, pp. 465–475.
Wells, P.R.A., 1977. Pyroxene thermometry in simple and complex systems. Contributions to Mineralogy and Petrology 62, 129–139.
Wilson, M., 1989. Igneous Petrogenesis. Chapman & Hall, London. pp. 1–466.
Wood, B.J., Banno, S., 1973. Garnet-orthopyroxene and orthopyroxene–clinopyroxene relationships in simple and complex systems. Contributions to Mineralogy and Petrology 42, 109–124.
Wood, B.J., Bryndzia, L.T., Johnson, K.E., 1990. Mantle oxidation state and its relationship to tectonic environment and fluid speciation. Science 248, 337–345.
Wood, B.J., Virgo, D., 1989. Upper mantle oxidation state: ferric iron contents of lherzolite spinels by ^{57}Fe Mössbauer spectroscopy and resultant oxygen fugacities. Geochimica et Cosmochimica Acta 53, 1277–1291.